MATHEMATICAL MODELING OF STRESS FIBER REORGANIZATION INDUCED BY CYCLIC STRETCH

A Thesis

by

HUI-JU HSU

Submitted to the Office of Graduate Studies of
Texas A&M University
in partial fulfillment of the requirements for the degree of

MASTER OF SCIENCE

August 2009

Major Subject: Biomedical Engineering

MATHEMATICAL MODELING OF STRESS FIBER REORGANIZATION INDUCED BY CYCLIC STRETCH

A Thesis

by

HUI-JU HSU

Submitted to the Office of Graduate Studies of
Texas A&M University
in partial fulfillment of the requirements for the degree of

MASTER OF SCIENCE

Approved by:

Chair of Committee, Roland R. Kaunas
Committee Members, Jay D. Humphrey
Emily Wilson
Head of Department, Gerard L. Cote

August 2009

Major Subject: Biomedical Engineering

ABSTRACT

Mathematical Modeling of Stress Fiber Reorganization Induced by Cyclic Stretch.

(August 2009)

Hui-Ju Hsu, B.S.; M.S., National Cheng Kung University

Chair of Advisory Committee: Dr. Roland R. Kaunas

Arterial endothelial cells (ECs) are subjected to pulsatile strain due to pressure changes in the cardiac cycle and this may play a significant role in vascular function in health and disease. Further, ECs differentially respond to different patterns of strain. There is much evidence that cyclic uniaxial strain results in a perpendicular orientation of ECs and their stress fibers, while no such alignment occurs in response to cyclic equaibiaxial stretch. It is unclear how cells and their stress fibers determine their specific response to particular spatiotemporal changes in the matrix, however. Given that ECs located at regions in the arterial tree prone to atherogenesis are non-aglined, while ECs in relatively healthy regions are oriented perpendicular to the principal direction of cyclic stretch, it is important to understand the mechanisms which regulate stretch-induced stress fiber alignment.

The focus of this thesis was to develop realistic models to describe the dynamic changes in the organization of stress fibers in response to diverse spatiotemporal patterns of stretch. The model is based on the premise that stress fibers are pre-stressed at a "homeostatic" level so that stress fibers are extended beyond their unloaded lengths, and that perturbation in stress fiber length from the homeostatic level destabilizes the stress

fibers. A deterministic model described experimentally measured time courses of stress fiber reorientation perpendicular to the direction of cyclic uniaxial stretch, as well as the lack of alignment in response to equibiaxial stretch. In the case of cyclic simple elongation with transverse matrix contraction, stress fibers oriented in the direction of least perturbation in stretch. Model analysis indicated the need for a time-dependent stress fiber mechanical property, however. Thus, a stochastic model was developed that incorporated the concept that stress fibers tend to self-adjust to an equilibrium level of extension when they are perturbed from their unload lengths with the turnover of stress fibers. The stochastic model successfully described experimentally measured time courses of stress fiber reorganization over a range of frequencies. At a frequency of 1 Hz, stress fibers predominantly oriented perpendicular to stretch, while at 0.1 Hz the extent of stress fiber alignment was markedly reduced and at 0.01 Hz there was no alignment at all. Both the deterministic and stochastic models accurately described the relationship between stretch magnitude and the extent of stress fiber alignment in endothelial cells subjected to cyclic uniaxial stretch. Parameter sensitivity analyses for each model were used to demonstrate the effects of each parameter on the characteristics of the system response. In summary, the mathematical models were capable of describing stress fiber reorganization in response to diverse temporal and spatial patterns of stretch. These models provide a theoretical framework to elucidate the mechanisms by which adherent cells sense the characteristics of matrix deformation and describe a mechanism by which the cells can then adapt to such deformations to maintain mechanical homeostasis.

ACKNOWLEDGEMENTS

I am extremely grateful to my advisor, Professor Kaunas R. Roland, for his vital encouragement and guidance throughout my graduate studies and research. His patience and enthusiasm in research had motivated me. In addition, he was always accessible and willing to help me with my research.

In addition to my advisor, I would like to thank the rest of my committee members, Professors Jay D. Humphrey and Emily Wilson, for their time in reviewing this thesis and for their thoughtful advice and feedback.

I also thank my fellow labmate, Chin-Fu Lee, for the experiment results that I used to compare with my simulations. He also inspires me in research through our interactions and discussions in the lab.

Last but not the least, my deepest gratitude goes to my family; most especially, my parents who spiritually supported me throughout my pursuit of a higher education.

TABLE OF CONTENTS

Page

Page

LIST OF FIGURES

Page

I. INTRODUCTION

I.A. Background

Endothelial cells (ECs) form a cell monolayer on the lumen of arteries to prevent the passage of macromolecules from the blood to the vascular tissue. ECs are continuously subjected to the hemodynamic forces - fluid shear stress and mechanical stress (Nerem 1993; Gimbrone 1999). These mechanical factors can be sensed by ECs to modify intracellular signaling, gene expression, and protein expression to regulate vascular functions such as vasoconstriction, platelet aggregation and smooth muscle cell proliferation. Importantly, mechanical forces play significant roles in atherosclerosis. Therefore, it is of considerable interest to clarify the effects of these mechanical factors on ECs and the detailed mechanisms by which ECs sense the mechanical forces.

Atherosclerotic lesions are primarily located at regions of arteries exposed to disturbed flow and excessive mechanical stress such as curves and the branch points in the arteries, resulting in EC dysfunction (Gimbrone 1999) and subsequent progressive plaque formation (Hahn et al., 2008). On the other hand, straight, unbranched arterial segments are largely devoid of plaques. The morphology of vascular endothelial cells (ECs) also varies in these locations in the arterial tree. Wall shear stress (WSS), the tangential drag force of blood flow passing the surface of endothelial cell, causes the endothelial cells to orient parallel to the direction of fluid flow in the straight region. In contrast, the oscillatory WSS at branches results in a lack of EC orientation (Chien 2008). Cyclic strain caused by pulsatile pressure is principally oriented in the circumferential direction

---

This thesis follows the style of *Journal of Theoretical Biology*.

in the straight, unbranched arteries, which leads to the orientation of ECs and their stress fibers in vivo perpendicular to the principle direction of stretch. On the other hand, the relatively non-directional stretch that occurs in the curves or the branch points of arteries does not caue ECs alignment (Chien 2007). The remodeling of EC structure in response to externally directed mechanical stimuli is therefore an important mechanism to minimize alterations in intracellular stress/strain (Chien 2007).

The structure of cultured ECs is dynamically changing not only in static condition but also in response to diverse temporal and spatial patterns of stretch. Several characteristics of the pattern of stretch on cell alignment have been examined, including uniaxial or equibiaxial stretch, stretch magnitude, and stretch rate. From previous studies (Kaunas et al., 2006; Wang et al., 2001), ECs and their actin stress fibers align perpendicular to the principal direction of cyclic uniaxial stretch, while ECs and their stress fiber do not align in a specific direction in response to cyclic equibiaxial stretch. The amplitude of cyclic stretch also affects the extent of stress fiber alignment (Wang et al., 2001; Kaunas et al., 2005; Wille et al., 2004). Both Kaunas et al. and Wille et al. demonstrated that an increase in the amplitude of cyclic stretch, ranging from 0 to 10 % stretch, results in the increase in the extent of alignment. Wang et al. (2001) concluded that the rate and extent of reorientation are determined primarily by the stretching magnitude, not stretching rate, and both the cell reorientation and stress fiber reorganization are specifically in the direction with minimum substrate deformation. However, there are accumulating studies on the role of frequency in the stretching-induced cell alignment (Liu et al., 2008; Jungbauer et al., 2008), demonstrating that strain rate is a key factor influencing cell alignment.

I.B. Existing Mathematical Models of Stretch-Induced Stress Fiber Orientation

Various groups have developed different mathematical models based on the experimental observations discussed above to describe the relationship between stress fiber reorientation and substrate deformation. Wang et al. (2000) proposed a mathematical model in which linearly elastic stress fibers undergo disassembly when their basal strain energy are perturbed beyond threshold values, resulting in the orientation of stress fibers in the direction of smallest normal strain in the matrix. Yamada et al. (2000) proposed a similar kinematic model assuming that a stress fiber aligns in the direction of the minimum changes in fiber length. Stress fiber remodeling is a gradual process, and these models cannot address the rate of stress fiber alignment. Further, remodeling involves the turnover of stress fibers. To account for the turnover of stress fibers, Na et al. (2007) proposed a rule-of-mixtures approach which describes the assembly and disassembly of individual constituents from a mixture of fibers in response to perturbed loads. Constrained mixture modeling has been successful in describing dynamic changes in the mechanical properties and organization of fibrillar extracellular matrix at the tissue scale in response to mechanical loading (Baek et al., 2005; Gleason and Humphrey, 2004; Humphrey and Rajagopal, 2003).

I.C. The Actin Cytoskeleton, Focal Adhesions, and Integrins

The details of mechanical stimulation from extracellular deformation leading to cytoskeleton reorganization and cell reorientation are not clear. However, certain cellular structures seem to be involved in the stress fiber alignment. Focal adhesions are the transmembrane proteins linking the extracellular matrix and the cytoskeleton via integrins (Burridge et al., 1988). Focal adhesions are found at each end of stress fibers; therefore, this mechanical link of integrins, focal adhesion, and stress fibers is able to transmit the matrix forces into the cell and vice-versa.

Stress fibers consist of bundles of actin filaments formed by the contractile interaction of actin and myosin. The contraction is isometric and uniform within individual ECs and between ECs under identical condition, causing ventral stress fibers to be prestretched to a level dependent on the level of contractile force (Lu et al., 2008; Deguchi et al., 2005b). Contractility involves activation of Rho small GTPase which induces myosin light chain phosphorylation to result in the formation of stress fibers and focal adhesions (Magdalena et al., 1996). When contractility is inhibited, integrins disperse from focal adhesions as stress fibers and focal adhesions disassemble. The extent of stretch-induced stress fiber alignment is affected by contractility (Kaunas et al., 2005; Chen et al., 2004; Wang et al., 2000).

Mechanical stretch of the matrix perturbs the level of fiber stretch from an equilibrium level, resulting in compensatory changes such as stress fiber turnover and reorientation (Kaunas et al., 2005; Wang et al. 2000; Chen et al. 2004). Individual stress fibers are thought to be actively tensed by the action of actomyosin motors and to function as

elastic cables that structurally reinforce the basal portion of the cytoskeleton (Lu et al., 2008; Deguchi et al., 2005b). Kumar et al. (2006) confirmed that stress fibers in living cells retract the severed ends at a rate of retraction described with a viscoelastic-type function. We hypothesized that stress fiber relaxation, turnover, and reorientation are the main mechanisms by which ECs and their stress fibers adapt to a change in matrix stretch.

I.D. Outline of the Thesis

Based on these observations, there is a clear need to better understand the mechanisms that regulate stretch-induced stress fiber reorganization. We have developed mathematical models, based on the rule of mixtures, which can accurately describe the kinetics of stress fiber turnover, with the rate dependent on the perturbation in fiber strain from a homeostatic level, in response to diverse patterns of stretch. This thesis describes two different mathematical models (deterministic and stochastic models) used to interpret stretch-induced stress fibers alignment. Each model is described as different sections of this thesis. Within each section, the Theory section describes the development of the model, including assumptions, initial conditions, kinematics, and kinetics of stress fiber turnover. In the Results section, a sensitivity analysis is performed to better understand the effects of each model parameter on the system behavior. Further, the model parameters are identified that provide the best model fitting to experiment data. The Discussion section provides interpretations of model simulation results. Finally, we provide an overall Discussion that critically evaluates model assumptions and provides predictions of future experiments that will provide further insight into stretch-induced stress fiber reorganization.

II. DETERMINISTIC MODEL*

II.A. Introduction

Cells tend to maintain constant certain mechanical variables such as stress fiber prestretch and focal adhesion stress. For instance, energy added to focal adhesions tend to increase the dissociation of focal adhesion proteins (Evans and Calderwood, 2007), suggesting that excessive tension increases the rupture of adhesion bonds. Lu and colleagues (Lu et al., 2008) reported that stress fiber are pre-extended to a level which is remarkably uniform within individual ECs and between ECs under identical conditions. Large stretches or compressions ($\pm 25\%$) perturb the level of stretch in the stress fibers, resulting in disruption of stress fibers. Moreover, precise measurements of forces generated at cell attachments indicate that cells tend to maintain constant the level of stress applied to focal adhesions (Balaban et al., 2001).

Together, these studies support the hypothesis that perturbing the stretch and/or tension in stress fibers and their associated focal adhesions above or below an optimum level tends to destabilize these structures.

Most of previous models successfully describe the orientation of stress fibers perpendicular to the direction of stretch, but do not address the rate of stress fiber alignment (Wang 2000; Yamada et al., 2000). As a result, only equilibrium behavior can be predicted by these models. Since the actin cytoskeleton inside cells is constant assembly and disassembly, there is a need to track the mechanical states in which these constituents are assembled and when they disassemble. Herein, a mathematical model is developed based on constrained mixture theory to describe the kinetics of stress fiber turnover and reorientation in response to diverse patterns of stretch. By expressing the rate of fiber disassembly using a rate constant dependent on the perturbation in fiber strain from the original stretch, deterministic model provides steady-state, as well as unsteady-state, solutions to the reorganization of stress fibers.

II.B. Method

The model described below was executed numerically in a Fortran program (See Appendix B).

II.B.1. Basic Assumptions

Initially, let us make the following assumptions for the mathematical models based on several experimental observations:

a. Well-spread cells are very flat in most areas except the nucleus. Further, large stress fibers in non-muscle cells are typically localized to the ventral surface of cell and are anchored at each end to the matrix via focal adhesions (Hotulainen and Lappalainen, 2006). Thus, we assumed that the actin cytoskeleton is 2D network, present in a narrow zone adjacent to the underlying extracellular matrix.

b. Isometric contraction formed by the contractile interaction of actin and myosin causes the ventral stress fibers to become prestretched to a level dependent on the level of contractile force (Lu et al., 2008). The level of stress fiber prestretch is remarkably uniform to ~10% within individual ECs and between ECs under identical conditions, suggesting that stress fiber prestretch is maintained at an equilibrium level. Hence, we propose that stress fibers are assembled in a prestretched state with a basal contractile tone in a magnitude $\alpha_0 = 1.10$.

c. The fiber network deforms in registry with the matrix. Consequently, the network of stress fibers is assumed to be constrained to move together with cells when the matrix deforms.

d. Matrix deformation can be characterized by normal and shear strains (Fung, 1994). Since stress fibers are essentially tensed cables anchored to the matrix via point-like focal adhesions, they are likely to only be subjected to normal matrix strains. Normal strain changes the distance between focal adhesions, hence changes the length of the associated stress fibers. Thus, normal substrate strain, not the shear substrate strain, determines the actin cytoskeleton reorganization (Wang, 2000).

e. The network of stress fibers will be treated as families of fibers that share the same orientation and the same reference configuration. The reference configuration is defined as the configuration of the stress fiber where the fiber no longer bears tension. Each individual family of fibers does not physically interact with each other or with other cellular components.

II.B.2 Initial Condition

The organization of stress fibers for individual unstretched cells is typically heterogeneous, which means there is no preferred direction for the stress fibers, on average, in a population cells. Let a representative "average" cell contain a uniform distribution of stress fibers along the ventral surface of the cell. Stress fibers are grouped into individual families of fibers that share the same orientation and the same reference configuration, which is defined as the traction-free configuration. For the simulations performed hereafter, the distribution of stress fibers is modeled as a discrete distribution with 5° intervals from -π/2 to π/2, rather than a continuous distribution. This limits the number of fiber families to a finite number. Further, let these newly assembled stress fibers all be prestretched to the same extent ($\alpha_0 = 1.10$).

II.B.3. Numerical Approximation of Matrix Stretch Patterns

Importantly, the reference configuration of a stress fiber is based on the current configuration of the matrix at the time of fiber assembly. When a smoothly changing stretch is applied to the matrix, a continuous spectrum of reference configurations would be generated, which is difficult to keep track of. Instead of a smoothly changing matrix stretch pattern, let us discretize the stretch pattern into *N* step changes in stretch of equal magnitude in order to limit the possible number of reference configurations to a finite number. The incremental stretch in the matrix can be described by the right Cauchy-Green tensor (*C*). For stretches lacking shear strain, the deformation gradient tensor (*F*) can be expressed as a diagonal matrix which the entries outside the main diagonal are all zero.

$$C = F^T F = \begin{bmatrix} {\lambda_1}^2 & 0 \\ 0 & {\lambda_2}^2 \end{bmatrix}, \text{ where } F = \frac{dx}{dX} = \begin{bmatrix} \lambda_1 & 0 \\ 0 & \lambda_2 \end{bmatrix} \quad (1)$$

where x is the current configuration of the matrix and X is the reference configuration. Here λ_1 and λ_2 are the two principal stretches in the directions of the orthonormal base. After a sequence of N incremental steps, the total deformation is equal to the following:

$$C_f = \prod_{i=1}^{N} C = \begin{bmatrix} {\lambda_1}^{2N} & 0 \\ 0 & {\lambda_2}^{2N} \end{bmatrix} \quad (2)$$

Each incremental stretch lasts for a time period adjusted to approximate time-varying stretch. For example, a sawtooth pattern of cyclic stretch with magnitude λ and frequency f can be approximated by a series of N incremental stretches of a constant magnitude $\lambda^{\frac{1}{N}}$, following by a series of N incremental stretches of a constant magnitude $\lambda^{-\frac{1}{N}}$. The sawtooth pattern of cyclic stretch is discretized into $2N$ incremental stretches per cycle with each incremental stretch maintained for a constant time interval $\Delta t = \frac{1}{2Nf}$. The stretch device we use to cyclically stretch cells generates a sinusoidal pattern of cyclic matrix stretch which can be approximated by varying the time interval with each cycle of stretch composed of 40 steps ($2N$ = 40) in total, as shown in Fig. 1A. We determined that the results of simulations of 10% cyclic uniaxial stretch at 1 Hz did not change when the value for N ranged from 10 to 100.

Based on constrained mixture theory, the deformation gradient for each stress fiber at time t, relative to its natural (pre-stretched) configuration, is $F^i_{n(\tau)}(t)$, is associated with mapping the points from the natural configuration of the constituent (produced at time $\tau\big(n(\tau)\big)$) to the current configuration at time t. The stretch in the fiber direction of the i^{th} constituent, relative to its original prestretched configuration, is given as

$$\alpha^i = \alpha_0 \alpha^i_{n(\tau)} = \alpha_0 \sqrt{M^i \cdot F^i_{n(\tau)}(t)^T F^i_{n(\tau)}(t) M^i} \quad (3)$$

where M^i is the unit vector in the direction of a fiber in its natural configuration.

II.B.4. Kinetics of Fiber Turnover

In this model, a deterministic approach similar to that used to describe chemical reaction kinetics is applied to model stretch-induced stress fiber turnover and subsequent reorganization. The i^{th} fiber family is defined as the stress fibers formed at the same time τ^i and oriented in the same direction. Each stress fiber exists until it is disassembled. Let us express the rate of fiber disassembly via first-order reaction kinetics,

$$\frac{d\phi^i}{\phi} = -k^i dt \quad (4)$$

where ϕ^i is the mass fraction of fiber family i and k^i is the rate constant for fiber disassembly.

A deviation of fiber stretch from its prestretched state, by either lengthening or shortening the matrix, increases the rate of stress fiber disassembly (Lu et al., 2008). Based on this observation, k^i was expressed as a function of the stretch of the fiber

$$k^i = k_0 \left[1 + k_1 \left(\frac{\alpha^i - \alpha_0}{\alpha_0}\right)^2\right] = k_0 \left[1 + k_1 \Delta\alpha^i\right] \quad (5)$$

where α_0 is the homeostatic level of stretch which corresponds to the prestretch generated in stress fibers when they are initially assembled, and $\Delta\alpha^i$ represents the normalized deviation of stress fiber stretch (hereafter referred to as fiber stretch) from the homeostatic stretch. The term in parentheses is squared to ensure that $\Delta\alpha^i$ is positive regardless of whether fiber stretch is larger or smaller than the homeostatic stretch.

For simplicity, we assume that the rate of fiber assembly equals the rate of disassembly such that the total mass fraction of stress fibers in the cell remains constant over time and is equal to the original total mass fraction before stretch.

$$\sum_{i=1} \phi^i(0) = \sum_{i=1} \phi^i(t) \tag{6}$$

Also, we assume stress fibers reassemble with equal probability in all directions. Consequently, we distribute the mass of disassembled stress fibers equally in all directions.

II.B.5. Quantify the Extent of the Stress Fiber Alignment by Circular Variance

The extent of the stress fiber orientation was determined by vectorially summing the individual orientation vector components, normalizing the result by the total number of vectors (*M*) and subtracting the obtained number from unity.

$$Circular\ Variance = 1 - \frac{1}{M}\sqrt{\left(\sum_{j=1}^{M} sin2\theta_j\right)^2 + \left(\sum_{j=1}^{M} cos2\theta_j\right)^2} \tag{7}$$

where θ_j is the angle for vector j. Circular Variance ranges from zero to unity, representing perfect alignment to a specific direction and a totally random distribution, respectively. Circular variance was computed from stress fiber orientation distributions in the simulations and the values were compared to values measured from images of phalloidin-stained stress fibers subjected to identical stretch conditions (e.g. 6 hr of 10% cyclic uniaxial stretch at 1Hz). Stress fiber orientation distributions were measured using an automated algorithm (see Appendix E for the code) based on pixel intensity gradients (Kaunas et al., 2005, 2006). For instance, the circular variance for a near-parallel distribution of stress fibers in a single cell, shown in Fig. 2A, is calculated to be 0.09.

II.B.6. Average Stress Fiber Stretch

Let the instantaneous mass-average fiber stretch ($\bar{\alpha}(t)$) be expressed as

$$\bar{\alpha}(t) = \frac{\sum_{i=1}^{N} \phi^i(t)\alpha^i(t)}{\sum_{i=1}^{N} \phi^i(t)} \tag{8}$$

II.B.7. Statistics

The best fitting parameters of this mathematical model to the experiment data is determined by minimizing a root mean sum of the squares of the error between measured values of circular variance and those predicted by the model. Regression analysis (Excel, Microsoft) was performed to calculate a R^2-value as a measure of the ability of the model to describe experimentally-determined time courses of circular variance. Oriana 2 circular statistics software (Rockware) was used to plot the circular histograms for the stress fiber orientations from experiments and simulations.

II.C. Results

We will first present simulation results illustrating the responses of the model to step and cyclic patterns of matrix stretch. Then we will present parameter sensitivity analyses to demonstrate the effects of the various model parameters on the system response. We will then estimate the values of model parameters from experimental data and then use these parameters to make predictions of stretch-induced stress fiber remodeling to various interesting stretch conditions.

II.C.1. Step Increase in Equibiaxial Stretch

The response to a step-change in equibiaxial stretch provides a clear demonstration of the role of stress fiber turnover dynamics (Fig. 3). Initially all the stress fibers are prestretched to a magnitude $\alpha_0 = 1.10$ before step-stretch on the matrix ($t < 0$). At $t = 0$, the matrix is stretched equally in all direction (i.e., $\lambda_1 = \lambda_2 = \lambda$ in Eq. (1)), and hence the stretch of stress fibers (α^i) becomes $\lambda\alpha_0$. According to Lu et al. (2008), releasing the prestretch or excessive stretching of a cell tends to induce stress fiber disassembly. These overly stretched stress fibers therefore disassemble at an accelerated rate (cf. Eqs. (4) and (5)) and immediately reassemble at the equilibrium stretch α_0 with the mass distributed equally in all direction. Since the stress fibers have two possible reference configurations – the original (α_0) and overly-stretched ($\lambda\alpha_0$) configurations, there are only two distinct families of actin fibers in this example. The time course of average fiber stretch can be computed using Eq. (8) and shown in Fig. 3B. Initially, the fiber stretch is $\lambda\alpha_0$ for all fibers, then the mass-average fiber stretch $\overline{\alpha} = \phi_0\alpha_0 + \phi_1\lambda\alpha_0$ returns to α_0 as all the overly stretched stress fibers are disassembly and replaced by new fibers with

basal contractile ($\alpha = \alpha_0$). The family of fibers at the original stretch also disassembles at the basal rate, but these stress fibers immediately reassemble at the same level of stretch. Consequently, only the overly stretched stress fibers have a net effect to result in a progressive return in average fiber stretch ($\bar{\alpha}_0$) to the original deposition stretch (α_0). The time required for the average fiber stretch to return from initial stretch ($\lambda\alpha_0$) to half of the deviation $\left(\alpha_0 * (\lambda - 1)\right)$ is defined as $t_{1/2}$ (Fig. 3B). The half life $t_{1/2}$ is shown as a function of the rate constant k^i (Fig. 3C). As a result of the stress fibers turnover, although the matrix remains stretched, the ECs adjust themselves to relax the fiber tension generated by matrix stretching.

II.C.2. Stress Fiber Organization in Response to Cyclic Equibiaxial and Uniaxial Stretch

Kaunas and colleagues (2006) have demonstrated distinctly different fiber orientation distributions in response to cyclic equibiaxial and uniaxial stretch shown in Figs. 4B and 4C. Cyclic uniaxial stretch (6 hrs, 1.1 stretch ratio, 1 Hz) induces stress fiber alignment perpendicular to the direction of stretch (Fig. 4B) while cyclic equibiaxial stretch does not (Fig. 4C). Simulations of these stretch conditions were performed and experimentally measured (Fig. 4A-C, right panels) and simulated stress fiber distributions (Fig. 4D-F) are compared. The stress fibers in confluent ECs are distributed uniformly in static control, as shown in Fig. 4A, which is assumed to be the initial condition of the mathematical model in the absence of perturbation in matrix stretch (Fig. 4D). The stress fibers of the static control are prestretched to a homeostatic state where $= \alpha_0$, which is substituted into Eq. (5) to result in a rate constant $k^i = k_0$ with no contribution from k_1 in

the absence of perturbation in matrix stretch. The stress fibers then disassemble at a basal rate as well as reassemble uniformly in all direction in the plane, therefore, the circular histogram of simulations of static control is uniform distribution (Fig. 4D). In response to cyclic uniaxial stretch, the stress fibers oriented parallel to stretch experience the high stretch perturbations and are consequently disassembled at the highest rates. Conversely, the stress fibers oriented perpendicular to stretch experience the lowest perturbations and are thus disassembled at the lowest rates (since $\Delta\alpha^i = 0$). While the rate of fiber assembly is equal in all directions, the rate of disassembly is clearly asymmetric. This results in the net accumulation of the stress fibers in directions of lowest perturbation in stretch (i.e., perpendicular to stretch) as shown in Fig. 4E. In contrast, the stress fibers subjected to cyclic equibiaxial stretch experience the same level of stretch in all directions, thus the disassembly rates are uniform in all directions. Consequently, the circular histogram of simulations of cyclic equibiaxial stretch is uniform (Fig. 4F). In summary, the model was capable of simulating the distributions of stress fiber orientations for static ECs and for ECs subjected to cyclic uniaxial and equibiaxial stretches.

II.C.3. Parameter Sensitivity Analysis

We perform a sensitivity analysis to better understand the effects of each model parameter, k_0, k_1, and α_0, on the system behavior.

II.C.3.a. The Roles of k_0 and k_1 on the Rate and Extent of Stress Fiber Alignment

By performing simulations of sinusoidal cyclic uniaxial stretch of amplitude 1.10 and frequency 1 Hz over a range of values for k_0 and k_1, the resulting curves are shown as a scaled figure in which circular variances are plotted versus non-dimensionalized time (tk_0) to clearly identify the role of k_0 and k_1 on the rate and extent of stress fibers alignment (Fig. 5). The rate of stress fiber alignment (i.e., rate of decrease in circular variance) is proportional to the rate of fiber turnover. Thus, for a given value of k_1, different values of k_0 (10^{-5} and $10^{-4}\,s^{-1}$) form a single curve in the non-dimensionalized plot (Fig. 5). As the mass fractions of the stress fibers that are oriented toward the direction of stretch decrease, their rates of disassembly also decrease (cf. Eq. (5)). The stress fiber distribution eventually reaches a steady-state condition where the time-integrated value of $k^i\phi^i$ over a cycle is equal in all directions. The rate of disassembly for stress fibers oriented parallel to stretch is $k^i = k_0\left[1 + k_1\Delta\alpha^i\right]$, while the rate of disassembly for fibers oriented perpendicular to stretch is $k^i = k_0$ (cf. Eq. (5)). The steady-state value for circular variance (i.e., the extent of stress fiber alignment) depends on the ratio of the rates of disassembly parallel and perpendicular to stretch ($1 + k_1\Delta\alpha^i$). Higher values of k_1 result in lower steady-state values of circular variance. Hence, the rate of stress fiber alignment is dependent on k_0 while the extent of stress fiber alignment is dependent on k_1.

II.C.3.b. The Relationship Between k^i and α^i

Motivated by observations that stress fibers disassembly quickly when they are either shortened or lengthened quickly, we developed an expression for the rate of fiber disassembly that increases proportionally to the deviation between the current and equilibrium level of fiber stretch (cf. Eq. (5)). The deviation is normalized by the value for equilibrium stretch and the result squared so that both negative and positive deviations result in elevated disassembly rates. The non-linear dependence between k^i and $(\alpha^i - \alpha_0)$ is not justified by any theoretical consideration, so we evaluated an alternative linear relationship where k^i is proportional to the absolute difference between the fiber stretch and the equilibrium value:

$$k^i = k_0 \left(1 + k_1 \left|\frac{\alpha^i - \alpha_0}{\alpha_0}\right|\right) \tag{9}$$

Fig. 6 shows that the time-courses of stress fibers alignment (i.e., changes in circular variance over time) are identical in the linear and nonlinear expressions (cf. Eqs. (9) and (5)). For obvious reasons, the optimal values of k_1 are different for these two expressions. Thus, it appears the results of the model will be similar whether Eq. (5) or (9) is used to describe the effect of fiber stretch on the disassembly rate. The nonlinear relationship (cf. Eq. (5)) was used for all the simulations described in this study.

II.C.3.c. The Value of Prestretch

There is accumulating evidence that altering the stress fiber pre-extension affects cell stiffness, morphology, locomotion and adhesion (Pelham and Wang, 1997; Polte et al., 2004). Therefore, pre-extension appears to be critical to stress fiber dynamics. Lu et al. (2008) and Deguchi et al. (2005b) reported stress fiber prestretch values of 1.10 and 1.26, respectively, in endothelial cells. Simulations performed using prestretch (i.e., the value of the homeostatic stretch) in the range from 1.1 to 1.3 indicated that the results are identical for any value of prestretch (data not shown).

II.C.4. The Rate Parameter Estimation for HUVECs and BAECs

The parameters were estimated from existing data in which stress fiber orientation distributions were quantified over time (Fig. 7). Only two such studies could be found in the literature. Yoshigi et al. (2003) measured stress fiber orientation in confluent human umbilical vein endothelial cells (HUVECs) subjected to uniaxial stretching (10%, 0.5 Hz) and presented the results as histograms of stress fibers orientation at different time points. I calculated circular variances for each time point and then performed simulations of 10%, 0.5 Hz cyclic uniaxial stretch with different values of k_0 and k_1 to fit the data. As illustrated in Fig. 7 (green curve), parameter values of $k_0 = 10^{-6}\ s^{-1}$ and $k_1 = 5.2 \times 10^5\ s^{-1}$ fit the data well ($R^2 = 0.82$).

Kaunas et al. (2006) measured the change in circular variance over time for confluent bovine aortic endothelial cells (BAECs) subjected to 10% cyclic uniaxial and equibiaxial stretches at 1 Hz. The rate parameters for the uniaxial data (Fig. 7, red curve) are $k_0 = 10^{-6}s^{-1}$ and $k_1 = 2.5 \times 10^5 s^{-1}$ ($R^2 = 0.85$). These values were also used to fit

the time points for equibiaxial stretch (Fig. 7, blue curve); however, the model predicts the circular variance of unity in response to equibiaxial stretch regardless of the values of the rate parameters. Thus, these results indicate that the mode is able to fit time courses for the circular variance in response to cyclic equibiaxial and uniaxial stretch using the same set of the rate parameters.

II.C.5. Model Predictions

II.C.5.a. The Effect of Changing the Direction of Stretch

Using the model parameters estimated from the data of Kaunas et al. (2006), the mathematical model was applied to predict the stress fiber reorganization as the direction of stretch changed. In the work of Kaunas et al. (2006), after 6 hr of 10% cyclic uniaxial stretch, the stress fibers align perpendicular to the direction of stretch. Changing the direction of stretch after the adaption of stress fibers to the original stretch direction resulted in a disruption of stress fiber orientation and the gradual realignment of the stress fibers perpendicular to the new direction of stretch. Noticeably, thirty minutes after changing the direction of stretch, the circular variance of the stress fibers was higher than before the change in stretch direction (Fig. 8, red circles); however, the stress fibers were still oriented perpendicular to the original direction of stretch. Six hours of additional stretch in the new direction, the stress fibers re-aligned perpendicular to the new direction of stretch. The model simulation predicts that the stress fibers achieve a uniform distribution in orientation (i.e., the value of circular variance is unity) after ~7 h (i.e., 1 h after changing the direction of stretch), and then the fibers proceed to orient away from the new direction of stretch. In addition, the simulation also predicts that the stress fibers

have aligned perpendicular to the new direction of stretch to an extent similar to that measured immediately before the direction of stretch changed.

II.C.5.b. Simulations Performed on Single-Cell Stress Fiber Distributions

Those simulations performed above assumed that the initial distribution of the stress fibers is uniformly based on a population of static cells, which leads to a value of unity for circular variance in static cells, which then rapidly decreases after initiating stretch. However, the stress fiber distributions within individual cells are varied from each other and usually have a preferred direction (cf. Fig. 4A), which results in the circular variance measured from experiment data being less than unity initially and have a lag time before it begins to rapidly decrease. Therefore, we perform simulations using the distributions of stress fibers which are measured from rhodamine-phalloidin stained images in individual cells under static conditions (Kaunas et al. 2006) as the initial conditions. When the initial distributions of the stress fibers within an individual cell is primarily oriented parallel to the direction of stretch, the fiber distribution gradually becomes less oriented until it is uniformly distributed (i.e., circular variance is unity), then it gradually orients perpendicular to the direction of stretch (Fig. 9A, blue, purple, orange and red lines). By contrast, if the original distribution of the stress fiber within an individual cells is primarily oriented in the direction perpendicular to stretch, the circular variance would decrease monotonically (Fig. 9A, green line). Importantly, the average of these simulation results in response to cyclic uniaxial stretch showing that the initial value of circular variance is not unity and that the initial rate of decrease in circular variance is not immediate (Fig. 9B). The stress fiber distributions invariably attain the same equilibrium distribution aligned perpendicular to the direction of stretch regardless of the initial

distribution of stress fibers (Fig. 9A). Thus, the differences between the simulations and experimental results may be attributed to the initial conditions imposed.

II.C.5.c. Effects of the Magnitudes of Stretch and RhoV14 Expression on the Estimation of k_1

Rho small GTPase is a key regulator of myosin activity and stress fiber formation. The interactive effects of changing the magnitude of stretch and the expression of constitutively-active Rho small GTPase (RhoV14) on stretch-induced stress fiber alignment in BAECs have been quantified (Kaunas et al., 2005). Specifically, different magnitudes of cyclic uniaxial stretch at 1 Hz for 6 hrs were applied to non-confluent BAECs which were either transfected with green fluorescent protein (GFP) as a control or co-transfected with GFP and the constitutively active mutant RhoV14. Only results at 6 hrs were measured, hence only the value of k_1 could be estimated from the data (Fig. 10). Consequently, the value of $k_0 = 10^{-6}s^{-1}$ determined above (cf. Fig. 7) was used in these simulations. Both sets of data were well described by the model using two different values for k_1 ($R^2 = 0.94$ and 0.97 for GFP and RhoV14/GFP cells, respectively). Cyclic stretching of BAECs co-expressing RhoV14/GFP led to a higher extent of stress fiber alignment (Fig. 10, red squares) compared to cell expressing GFP alone (Fig. 10, blue triangles). Consequently, the estimated values of k_1 for the RhoV14/GFP cells ($k_1 = 1.6 \times 10^5 s^{-1}$, Fig. 10, red curve) is larger than for GFP cells alone ($k_1 = 4.0 \times 10^5\ s^{-1}$, Fig. 10, blue curve).

II.C.5.d. Time Evolution of Fiber Stretch

Based on the turnover of actin stress fibers, this model predicts the evolutions of average fiber stretch ($\bar{\alpha}(t)$, cf. Eq. (8)) in response to different pattern of cyclic stretch (Fig. 11). In the case of cyclic equibiaxial stretch of magnitude $\lambda^N = 1.1$, all the stress fibers have the same reference configuration initially and the initial value of fiber stretch, $\bar{\alpha}(t)$, oscillates between α_0 and $\alpha_0\lambda^N$ as the matrix stretches between the original and fully-deformed configurations (Fig. 11A, blue curve). Over several cycles of stretching, the values of fiber stretch, $\bar{\alpha}(t)$, gradually decrease until the steady-state values are reached where $\bar{\alpha}(t)$ oscillates between $2\alpha_0/(\lambda^N + 1)$ and $2\alpha_0\lambda^N/(\lambda^N + 1)$ then the matrix stretch is between the original and fully-deformed configurations, respectively. Thus, although the absolute values of $\bar{\alpha}(t)$ gradually decrease until the steady-state is reached, the amplitude of fiber stretch (i.e., ratio of maximum to minimum values of $\bar{\alpha}(t)$ over a cycle) remains constant, λ^N, for $t > 0$. The gradually decrease in the values of fiber stretch is due to the disassembly of the original stress fibers and the subsequent reassembly of new stress fibers with reference configurations different from that of the original stress fibers. Before stretching ($t < 0$), all stress fibers are unstretched and their reference configurations are based on the unstretched matrix configuration. After the matrix stretches ($t > 0$), some stress fibers disappear and immediately reappear with reference configurations which are based on the current configuration of the stretched matrix at the time the stress fiber is assembled. For example, if a stress fiber is assembled when the matrix is in the fully deformed configuration, the fiber stretch ratio will decrease to $\frac{\alpha_0}{\lambda^N}$ as the matrix returns to its original unstretched configuration. Over time, when a steady-state is reached, the reference configurations of stress fibers become

uniformly distributed over the range of matrix configuration. Unlike the case of a step change in equibiaxial stretch, stress fibers do not all return to their original configurations to relax the tension generated by cyclic equibiaxial stretch. Instead, fiber stretches are continues perturbed from α_0 as long as the matrix continues to be cyclically stretched. However, in the case of cyclic uniaxial stretch, this model predicts a significant difference in the evolutions of average fiber stretch, which results in the alignment of stress fibers. The initial value of fiber stretch, $\bar{\alpha}(t)$, oscillates between α_0 and $\alpha_0\alpha_s(\theta)$, where $\alpha_s(\theta)$ is the component of fiber stretch contributed by matrix stretching, as the matrix stretch between original and fully deformed configuration (Fig. 11A, red curve). The average value for $\alpha_s(\theta)$ is

$$\langle\alpha_s(\theta)\rangle = \int_0^{\pi} \sqrt{\lambda^{2N}\cos^2\theta + \sin^2\theta}\, d\theta \approx 0.955\lambda^N \tag{10}$$

Hence, fiber stretch, $\bar{\alpha}(t)$, initially oscillates between $\alpha_0 = 1.10$ and $\alpha_0 0.955\lambda^N \approx 1.156$ (vs. 1.21 for equibiaxial stretch of $\lambda^N = 1.1$). Since stress fibers reorient in the case of cyclic uniaxial stretch, stress fibers accumulate in the direction of minimum perturbation in stretch, causing the amplitude of oscillate in fiber stretch for cyclic uniaxial stretch to be smaller than that for cyclic equibiaxial stretch. Moreover, unlike the case of cyclic equibiaxial stretch, the amplitude of oscillation continues to decrease slowly even when a steady-state of cyclic equibiaxial stretch is reached.

In summary, the mathematical model predicts the adaption of stress fiber in response to cyclic uniaxial stretch by reducing the perturbation in fiber stretch, while fiber stretch is sustained in response to cyclic equibiaxial stretch.

II.C.5.e. Time Evolution of Fiber Turnover Rate

In addition to the difference in the time evolution of fiber stretch between cyclic uniaxial and equibiaxial stretch (Fig. 11A), the model predicts a difference in the time evolution of fiber turnover rate as well (Fig. 11B). The rate of fiber disassembly ($\sum d\phi^i/dt$) is tracked over time in response to matrix stretch. For the simulation of cyclic stretch, the rate of fiber turnover was computed as the total amount of fiber disassembled over a cycle of stretch (i.e., the summation of fiber disassembled over 2N steps from the time matrix stretch in the original configuration) divided by the duration of a cycle. For 10% cyclic stretch, the simulation results are different in response to uniaxial and equibiaxial stretch (Fig. 11B). Before stretching (t<0), all stress fibers are in the unstretched matrix configuration, resulting in a basal rate of fiber disassembly without the effect of deviation from homeostatic level of stretch (i.e., $k^i = k_0$). After the matrix stretches, stress fibers in all directions are perturbed from their homeostatic level of stretch, which cause an initial step increase in the disassembly rate of stress fibers. As soon as some stress fibers disassembly and immediately reassembly with reference configuration depending on the current configuration of the stretched matrix, fiber turnover rate gradually decays as the values of fibers stretch decrease. A steady-state turnover rate for cyclic equibiaxial stretch is reached as the fiber reference configuration is uniformly redistribution over the entire range of matrix configurations (Fig. 11B, blue curve). In contrast, due to the asymmetry of stretch in the case of cyclic uniaxial stretch, stress fibers in the parallel direction of stretch have the highest disassemble rate while stress fibers in the perpendicular direction of stretch only have the basal disassemble rate. Thus, the rate of fiber disassembly is smaller in the case of cyclic uniaxial stretch than in

the case of cyclic equibiaxial stretch. In addition, due to the orientation of stress fibers, the turnover rate for cyclic uniaxial stretch continues to decay until return to the baseline level as the stress fibers become aligned perpendicular to the direction of stretch (Fig. 11B, red curve).

In summary, the model predicts that the alignment of stress fibers results in a transient increase in the rate of fiber turnover in response to cyclic uniaxial stretch, while the lack of a preferred orientation of stress fibers cause a sustained in the rate of fiber turnover in response to cyclic equibiaxial stretch.

II.C.6. Cyclic Stretch with Lateral Contractions

In the previous sections, uniaxial stretch is generated by restraining lateral contraction (cf. $\lambda_1 > 1$ and $\lambda_2 = 1$ in Eq. (1)). In this section, a simple elongation is generated by relaxing the restriction on contraction transverse to the direction of elongation (cf. $\lambda_1 > 1$ and $\lambda_2 < 1$ in Eq. (1)).

Previous studies have shown that stress fibers were arranged at a specific oblique angle relative to the direction of stretch when the cells were subjected to a simple elongation (Takemasa et al., 1997; Wang, 2000). Wang (2000) proposed that stress fibers tend to form in the direction of minimum normal strain, which depends on the Poisson ratio (ν) for the matrix.

$$\theta = \cos^{-1}\sqrt{\frac{\nu}{1+\nu}} \tag{11}$$

where $\nu = -\frac{1-\lambda_2}{1-\lambda_1}$. Two different ratios ($\nu = 0.35$ for silicon rubber and $\nu = 0.5$) were simulated and compared with previous studies. After 6 hrs of 10% cyclic simple stretch, our model predicted that stress fibers predominately oriented at $\pm 60°$ and $\pm 55°$ relative to the principle direction of stretch for the Poisson ratios of 0.35 and 0.5, respectively (Fig. 12A and Fig. 12B, respectively). These simulation results are the same as those predicted by Eq. (11).

II.D. Discussions

The results of this section indicate that a kinetic model based on constrained mixture theory is able to describe the reorganization of actin stress fibers in adherent cells in response to diverse patterns of mechanical stretch. Previous studies support the concept that cells seek to maintain a constant level of fiber stretch and that perturbing the level of stretch from this optimal level destabilizes the fiber (Lu et al., 2008; Takemasa et al., 1997). Previous models have successfully described the orientation of stress fibers after several hours of cyclic stretch, i.e. at equilibrium (Wang, 2002; and Takemasa 1998). By expressing the rate of fiber disassembly using an expression dependent on the perturbation of fiber stretch from the set point (cf. Eqs. (4) and (5)), the model describes both the equilibrium and transient reorganization of stress fibers. In the case of cyclic uniaxial stretch, the asymmetry of stress fiber disassembly and immediate uniform redistribution of the actin mass results in an accumulation of stress fibers in the direction of smallest normal matrix stretch (i.e., perpendicular to the direction of stretch), as shown in Fig. 4E. In contrast, stress fibers do not reorient in response to cyclic equibiaxial stretch (cf. Fig. 4F) since there is no direction of smallest normal matrix stretch.

Parameter sensitivity simulations were performed over a range of values for the parameters k_0 and k_1 to illustrate the effect of each parameter on the system behavior. The results indicate that the rate of stress fiber alignment is dependent on the values of k_0, while the extent of stress fiber alignment is determined by k_1 (cf. Fig. 5). The model accurately describes the relationship between stretch magnitude and the extent of stress fiber alignment in non-confluent BAECs which are either transfected with green fluorescent protein (GFP) as a control or co-transfected with GFP and the constitutively

active mutant RhoV14 in response to cyclic uniaxial stretch. The effect of RhoV14 expression is predicted as an increase in k_1 from 1.6×10^5 to 4.0×10^5 s^{-1} since the expression of RhoV14 increases contractility, resulting in an increase in the extent of stress fiber alignment induced by a given amplitude of cyclic uniaxial stretch in BAECs (cf. Fig. 10). The parameter k_1 characterizes the sensitivity of the stress fiber disassembly rate to perturbations in stretch (cf. $\Delta\alpha^i$ in Eq. (5)). Deguchi et al. (2005b) has reported that raising the basal fiber stretch increases the modulus of the stress fiber, thus amplifying the generation of stress for a given level of stretch. The strain hardening behavior of stress fibers may be able to explained the increase in sensitivity of stress fiber disassembly since relatively larger stress can be transmitted to focal adhesions proteins to induce de-adhesion, or the stress may induce direct disassembly of the stress fibers themselves to result in an increase in stress fiber disassembly.

Stress fiber stiffness has been shown to increase with increasing fiber stretch (Deguchi et al., 2005b). Consequently, the predicted changes in fiber stretch can be used to predict changes in cell stiffness in response to different patterns of stretch. In the case of a step change in matrix stretch, the model indicated a step increase in average fiber stretch initially followed by a gradual return back to the original equilibrium value. Therefore, it is expected that a step in stretch will cause a transient increase in cell stiffness. Based on this model, the stress relaxation is a result of stress fiber turnover, which does not require intrinsic viscoelastic behavior of the individual stress fibers. Thus, this is the first model described in terms of stress fiber kinematics without needing to specify a constitutive relationship between fiber stress and strain to accurately predict the dynamic changes in cellular mechanical properties in response to diverse patterns of matrix.

Previous studies reported that the orientation of ECs and their stress fibers depends on the amplitude of stretching (Kaunas et al., 2005; Wilke et al., 2001; Takemasa et al., 1997). Increasing the externally applied cyclic stretch results in an increase in the perturbation of fiber stretch from the set-point (Eq. (5)), hence elevating the disassembly rate of stress fibers parallel to the direction of cyclic uniaxial stretch. Consequently, the model predicts that more stress fibers accumulated in the direction of smallest normal matrix stretch and the extent of stress fiber alignment increases with increasing the amplitude of stretching.

Wei et al. (2008) have proposed a kinetic model of stretch-induced stress fiber remodeling which describes several of the same results of deterministic model: the magnitude-dependent alignment of stress fibers perpendicular to the direction of cyclic uniaxial stretch; the lack of stress fiber alignment induced by cyclic equibiaxial stretch; and the change in stress fiber orientation in response to a change in the direction of cyclic uniaxial stretch. There are several important distinctions in their model compared to ours. First, they presumed that cells are initially devoid of stress fibers and only begin to assemble stress fibers under cyclic stretch conditions. Second, they predict that the rate of stress fiber growth is greatest in the directions with least matrix shortening, such as occurs during the retraction phase of a matrix stretch cycle. Third, their approach is based on linear strain theory, which is not valid for the relatively large (10%) strains used in their simulations. Fourth, their model predicted that stress fiber alignment occurs within 10 min in response to 10% cyclic uniaxial stretch while the stress fiber alignment typically occurs over a course of hours (Kaunas et al. 2005, 2006). Finally, their model predicts that stress fiber concentrations are lower in cells subjected to cyclic equibiaxial

stretch compared to the uniaxial stretch case, which is not observed experimentally (Kaunas et al., 2006).

In summary, the model describes the general characteristics of stretch-induced stress fiber dynamics in experimental data. This simple model is not suggested to describe the complex reorganization of actin filaments within individual cells such as cortical meshworks. The model predicts that the rate of stretch-induced stress fiber disassembly determines the rate of alignment, and that stress fibers tend to orient toward the direction of minimum matrix stretch where the rate of stress fiber turnover is a minimum. Constrained mixture modeling has been successful at describing dynamic change in mechanical properties and organization of fibrillar extracellular matrix at the tissue-scale in response to mechanical load (Baek et al., 2006; Gleason and Humphrey 2004; Humphrey and Rajagopal, 2003). This thesis provides results supporting that the constrained mixture theory also applies to cell-scale fibrillar protein remodeling. Thus, the constrained mixture approach has the potential to describe vascular mechanics at length-scales ranging from the intracellular to whole tissue levels. Recently, Jungbauer and colleagues (2008) reported that cells are sensitive to stretch in the range of 0.01 to 1 Hz. Thus, we performed the simulation of the relationship between the frequency of stretch and the extent of stress fiber reorientation (Fig. 13). The model was found to predict that cells were sensitive to stretch over a range of frequencies of 10^{-6} to 10^{-4} Hz, suggesting a need to refine the model. Consequently, a stochastic model is addressed in the next section to better describe the effect of strain rate by incorporating time-dependent material properties to the stress fibers.

III. STOCHASTIC MODEL[†]

III.A. Introduction

In the Section II, we developed a mathematical model in which stress fiber alignment perpendicular to the stretch direction occurs as a consequence of the accelerated disassembly of stress fibers whose level of extension is perturbed from a set-point level. The gradual reorganizations of stress fibers in ECs subjected to cyclic uniaxial and (lack of reorganization for) equibiaxial stretch were well described over time using this model. It is worth noting that the deterministic model only described mechanical state of stress fibers in terms of kinematics, thus avoiding having to specify a constitutive relationship between fiber stress and strain. The constitutive behavior of stress fibers in intact cells is complex and remains to be elucidated. Several studies indicate stress fibers are not simply elastic filaments, but instead show viscoelastic behavior. Kumar et al. (2006) described measured rates of retraction of the severed ends of individual stress fibers in living cells using a viscoelastic-type function, represented schematically as a spring and dashpot in parallel. Motivated by these studies, we developed a new version of our model that evaluates the respective roles of the rates of stress fiber self-adjustment as a mechanism to modulate the response of stress fiber networks to different frequencies of cyclic stretch.

There is accumulating evidence that stress fiber alignment in response to cyclic stretch depends on the frequency of stretch (Liu et al., 2008; Jungbauer et al., 2008). As described below, there is a threshold frequency of 0.01Hz below which no alignment is

[†]Reprinted with permission from "A Dynamic Stochastic Model of Frequency-Dependent Stress Fiber Alignment Induced by Cyclic Stretch" by Hui-Ju Hsu, Chin-Fu Lee, Roland Kaunas, 2009. *PLoS ONE*, 4, e4853. Copyright [2009] by Open Access.

observed (Section III.C.1). The deterministic model developed in Section II predicts a threshold frequency for stress fiber alignment on the order of 10^{-6} Hz, indicating a clear need to modify the model. In this section, the self-adjustment of stress fiber stretch in response to the perturbation of stretch will be incorporated into stochastic model as a viscoelastic-type expression. In addition, we now employ a stochastic approach which allows several assumptions to be relaxed such as the necessity for stress fibers to only have orientations and stretch ratios within discrete ranges. Further, the fate of individual fibers are tracked over time (i.e., each fiber is its own "family").

First, we will present simulation results showing the effect of stretch frequency on the stretch-induced stress fiber alignment, which are used to estimate the optimized parameters by fitting the time-course of experiment data. Then a sensitivity analysis is performed to better understand the effects of each model parameters on the system behavior. The optimized parameter is used to demonstrate the ability of the model to predict several interesting characteristics of the responses to cyclic uniaxial and equibiaxial stretch at different frequencies and to predict the effects of stretch magnitude on stress fiber alignment.

III.B. Method

The model described below was executed numerically in Visual C++ (See Appendices C and D).

III.B.1. Basic Assumptions

The same assumptions from Section II.B.1 were used to develop the stochastic model, with the additional assumptions which are listed in below:

a. The total number of stress fibers in the simulation is assumed to be 1000. We found that increasing the number reduced the noise in the circular variance curves, but the system response was identical.

b. The sinusoidal pattern of cyclic stretch with magnitude λ and frequency f is discretized into 2N incremental stretches per cycle with variably incremental stretch maintained for a constant time interval $\Delta t = 1/(2Nf)$, shown in Fig. 14.

c. Instead of uniform reassembly in all direction for deterministic model, let us assume that stress fibers reassemble in a random oriention after disassembly in stochastic model.

III.B.2. Initial Condition

As described in Section II.B.2*,* stress fibers inside a population of unstretched ECs have no preferred direction. Consequently, let us assume that each cell contains a distribution of fiber orientations where each orientation is randomly chosen from a uniform and continuous distribution between 0 and 180°. Note that we now relax the constraint that fibers must be distributed into 5° intervals.

III.B.3. Dynamics of Fiber Turnover

Given the need to follow the assembly and disassembly of individual stress fibers and the mechanical states in which these fibers are formed, we had initially modeled the turnover of stress fibers by mass-action kinetics using the usual deterministic approach (cf. Eq. (4)). The results of deterministic model provide a population-averaged behavior, but are not meant to accurately describe individual stress fiber dynamics in cells. The response of an individual stress fiber is considered as a random event, similar to the roll of a die. If repeated many times the sequence of random events will exhibit certain statistical patterns, which can be studied and predicted. As a mathematical foundation for statistics, probability theory is essential to relate the microscopic properties of individual stress fibers to the macroscopic of a population of stress fibers that can be observed in cells. Hence, the turnover of individual stress fibers is expressed in terms of probabilities in the stochastic model.

For the stochastic model, the probability that a particular stress fiber, existing at time *t,* will disassemble at time $t + \Delta t$ is

$$P(\text{disassembled}, t + \Delta t \mid \text{assembled}, t) = k^i \Delta t \tag{12}$$

where k^i is defined as a function of the fiber stretch perturbation from the homeostatic level, as shown in Eq. (5) in Section II.B.4.

The fate of each fiber is determined by integrating Eq. (12) over time until the condition $P < k^i \Delta t$ is satisfied and the fiber disassembles. This same integration is performed for each fiber simultaneously. The numerical integrations were performed using a time increment Δt of 0.01 s. In test cases, decreasing Δt below 0.01 s did not significantly change the results of the simulation.

III.B.4. Self-Adjustment of Stress Fiber Extension

Lu and colleagues (2008) demonstrated that the intrinsic control of pre-extension in stress fibers is sufficiently robust that pre-extension is the same even after stress fibers have been disrupted and reorganized. Kumar et al. (2006) measure the retraction kinetics of the severed ends of individual stress fibers in living cells and described the rate of retraction using a viscoelastic-type function, represented schematically as a spring and dashpot in parallel.

Motivated by these studies, let us assume the stretch ratio of stress fibers following by a perturbation of magnitude ($\alpha^i - \alpha_0$) gradually returns to the homeostatic level of stretch.

$$\alpha^i = \alpha_0 + (\alpha^i - \alpha_0) exp\left(-\frac{t}{\tau}\right) \tag{13}$$

where τ is the characteristic time for the return of fiber stretch to the equilibrium value.

III.B.5. Quantify the Extent of the Stress Fiber Alignment by Circular Variance

(Please refer to Section II.B.5)

III.B.6. Average Stress Fiber Stretch

(Please refer to Section II.B.6)

III.B.7. Statistics

(Please refer to Section II.B.7)

III.C. Results

III.C.1. Dependence of Stress Fiber Alignment on Stretch Frequency

Stretch experiments show that the alignment of ECs depends on the frequency of stretching (Hsu et al, 2009). Non-confluent BAECs were subjected to 4 hr of 10% cyclic sinusoidally-varying uniaxial stretch at frequencies of 0.01 Hz (Fig. 15A), 0.1 Hz (Fig. 15B), and 1 Hz (Fig. 15C). The distributions in stress fiber orientations at different frequencies are compared for experimentally measured (Fig. 15A-C, left panels) and simulated (Fig. 15D-F) experiments. The simulations were performed using the optimized parameters identified below (Section III.C.3). At frequency of 0.01 Hz, the stress fibers lack any preferred orientation and are distributed randomly (Fig. 15A and D) , while at frequency of 0.1 Hz (Fig. 15B and E) and 1 Hz (Fig. 15C and F), the stress fibers oriented perpendicularly with the extent of alignment noticeably higher for 1 Hz.

III.C.2. Parameter Sensitivity Analysis

Similar to Section II.C.3, a sensitivity analysis was performed to clarify the roles of each model parameter on the system response.

III.C.2.a. The Roles of k_0 and k_1 on the Rate and Extent of Stress Fiber Alignment

Simulations were performed of 10% cyclic uniaxial stretch at 1 Hz over a range of values for k_0 and k_1 by fixing $\tau = 0.5\ s$, which is the optimized value determined below (Section III.C.3). To illustrate the effect of the value of k_0 on the rate of stress fiber alignment, circular variance was plotted versus a scaled time tk_0 (Fig. 16A). Different values of k_0 (10^{-5} and $10^{-4}\ s^{-1}$) form identical time-scaled curve for a given value of

k_1. On the other hand, for a given value of k_0, increasing the value of k_1 results in a decrease in the steady-state value for circular variance. Thus, k_0 determines the rate of stress fiber alignment, while k_1 determines the extent of stress fiber alignment.

III.C.2.b. The Role of τ on the Rate of Stress Fibers Self-Adjustment

The effect of the rate of stress fiber self-adjustment was analyzed by varying the value of the time constant τ while fixing the other two parameters k_0 and k_1 at their optimal values determined below (Section III.C.3, $k_0 = 3.0 \times 10^{-4}\, s^{-1}$ and $k_0 = 1.7 \times 10^{4}\, s^{-1}$). The steady-state average value for circular variance was plotted versus a scaled frequency, $\tau\omega$ (Fig. 16B). The steady-state circular variance is a sigmoid-like function of scaled frequency for τ values ranging from 0.005 to 0.5 *s*. When the scaled frequency is below a threshold value 0.005, stress fibers do not aligned in response to cyclic stretch. Conversely, when the scaled frequency is above 0.5, the steady-state circular variance reaches a minimum value and increasing the frequency further does not increase the extent of alignment. Thus, stretch-induced alignment is sensitive to stretch frequency over a range of two orders of magnitude.

III.C.3. The Rate Parameter Estimation for BAECs

The parameter estimation of this model was determined by fitting the experimental results (Fig. 15A-C) in which the stress fiber orientation distributions were measured as a function of time at frequencies of 0.01, 0.1, and 1 Hz (Fig. 17, black squares, blue triangles, and red circles, respectively). At 0.01 Hz, the measured circular variances is maintained near unity, while at 0.1 and 1 Hz, the circular variances gradually dropped during the first 2 hours of stretch before reaching a steady state. Simulations were

performed for 10% cyclic uniaxial stretch at frequencies of 0.01, 0.1, and 1 Hz (Fig. 17, black, blue, and red curve, respectively). The least-squares fitting between the time courses of circular variance determined by simulation and the experimental data (Section III.B.4*)* was used to identify the optimized model parameters ($\tau = 0.5\ s, k_0 = 3.0 \times 10^{-4}\ s^{-1}$ and $k_0 = 1.7 \times 10^{4}\ s^{-1}$). The model describes the distribution of stress fibers by angular histogram (Fig. 15D-F) and in the time-course of stress fiber orientation by circular variance (Fig. 17) for all three sets of data. However, the simulation predicted the stress fibers align more quickly than the experiment data at 1 Hz.

III.C.4. Model Predictions

III.C.4.a. Time Evolution of Fiber Stretch Amplitude in Response to Cyclic Uniaxial Stretch

In this section we evaluate the respective roles of the rates of stress fiber turnover and self-adjustment as mechanisms to modulate the response of stress fiber networks to different frequencies and magnitudes of cyclic stretch. In the absence of stress fiber turnover and self-adjustment, all the stress fibers would have the same reference configuration based on the unstretched matrix configuration. Thus, the instantaneous population-average fiber stretch (α_{avg}) would be expected to oscillate between the basal fiber stretch ($\alpha_0 = 1.10$) and a maximal value (1.155) corresponding to the original and the fully deformed state of matrix stretch, respectively. However, if the turnover and self-adjustment of stress fibers are considered, α_{avg} changes over time (Fig. 18A).

In the case of 10% cyclic uniaxial stretch at 1Hz, the initial value of α_{avg} oscillates between 1.10 and 1.155; however, within seconds, the maximum and minimum values

for α_{avg} drop to 1.078 and 1.122 so that the time-averaged value of α_{avg} is equal to α_0 (Fig. 18A, red curves). This initial drop in fiber stretch is completely attributable to the self-adjustment of stress fibers, which causes the time-averaged value of fiber stretch for each individual fiber to decay to α_0 within a characteristic time τ. While the time-average fiber stretch decreases almost immediately, the amplitude of the instantaneous population-average fiber stretch (i.e., ratio of maximum to minimum values of α_{avg} over a cycle) only slowly decreases as a result of the gradual reorientation of stress fibers toward the direction of least perturbation in normal matrix strain (i.e., perpendicular to the direction of cyclic stretch). The alignment occurs because the stress fibers in the direction of stretch experience the largest perturbation from set-point levels of stretch (α_0) resulting in higher probability of disassembly (cf. Eq. (12)), therefore, an accumulation of fibers occurs in the perpendicular direction of stretch (cf. Fig. 15C).

At 0.01 Hz, the instantaneous population-average fiber stretch (α_{avg}) does not vary despite the fact that the matrix is stretching (Fig. 18A, black curves), while the amplitude of α_{avg} at 0.1 Hz stretch is at an intermediate amplitude (Fig. 18A, blue curves). Thus, the amplitude of fiber stretch depends on stretch frequency because the stress fibers dissipate more strain when strain rates are relatively low. This provides an explanation for the lack of fiber alignment at low stretch frequencies since reducing the asymmetry in α_{avg} (i.e., the ratio of maximum to minimum values of α_{avg} over a cycle), as occurs at lower frequency, reduces the stimulus for stress fiber alignment.

III.C.4.b. Time Evolution of Fiber Turnover Rate in Response to Cyclic Uniaxial Stretch

Another characteristic predicted to be affected by stretch frequency is the rate of turnover of stress fibers. Similar to Section II.C.5.e, the rate of fiber turnover was computed as the total number of fiber disassembled over a 100-second period of stretch divided by the time period duration. From Eq. (12), the probability of stress fiber turnover is dependent on the rate constant k^i which is proportional to the deviation of fiber stretch from the equilibrium value α_0. Consequently, the rate constant for stress fiber disassembly is highest when the deviation of fiber stretch is highest, which is immediately after initiating cyclic stretch. For 1 Hz cyclic uniaxial stretch, the drop in fiber stretch amplitude after matrix stretch results in a gradually decrease in stress fiber turnover rate until the steady-state average value of circular variance is reached (Fig. 18B, red curve). For 0.01 Hz cyclic uniaxial stretch, the rate of stress fiber turnover remains at the basal level at all times because of fiber stretch amplitude is essentially zero even though the matrix is stretching (Fig. 18B, black curve), while an intermediate response is observed at 0.1 Hz (Fig. 18B, blue curve).

III.C.5. Effect of Cyclic Equibiaxial Stretch

Previous studies (Wang et al., 2001; Kaunas et al., 2006) show that, in contrast to cyclic uniaxial stretch, there is no stress fiber alignment in response to cyclic equibiaxial stretch (Fig. 4). The stochastic model predicted that cyclic equibiaxial stretch at any frequency does not result in the preferred orientation of stress fibers in any particular direction since there is no asymmetry in stress fiber stretch (Fig. 19A). Similar to the

prediction for cyclic uniaxial stretch, the average fiber stretch is dependent on stretch frequency (Fig. 19B). Specifically, smaller fiber stretch amplitudes are generated at lower stretch frequencies. However, since stress fibers cannot orient in a direction of minimum matrix normal strain, the amplitude of fiber stretch does not decrease (Compare Fig. 18A and 19B). Thus, a sustained elevation in the amplitude of fiber stretch results in a sustained upregulation of stress fiber turnover rate, which is dependent on the frequency of stretch as well (Fig. 19C). Consequently, the stochastic model predicts that stress fibers responses to different frequencies are due to the self-adjustment of stress fibers.

III.C.6. Effect of Uniaxial Stretch Magnitude

The optimized parameters estimated in Section III.C.2. (i.e., $\tau = 0.5\ s, k_0 = 3.0 \times 10^{-4}\ s^{-1}$ and $k_0 = 1.7 \times 10^{4}\ s^{-1}$) were used to predict the relationship between stress fiber alignment and the magnitude of cyclic uniaxial stretch at 1 Hz. Since the alignment of stress fibers occurs before 4 hr at frequency of 1 Hz, the steady-state value of circular variance in simulation is defined as the average value of circular variance after 6 hr. The steady-state value of circular variance decreases when the stretch magnitude increases, which is similar to the experimental measurements by Kaunas et al. (2005) (Fig. 20). It should be noted that if the simulation of parameter optimized is performed for this set of data, the stochastic model would provide a better fit. By using the parameters optimized for the test data set (cf. Fig. 17), the simulation results illustrate the ability of the model to predict the effect of stretching magnitude on stress fiber alignment.

III.D. Discussions

The results in this section indicate that ECs and their stress fibers can adapt to cyclic uniaxial stretch via two distinct mechanisms – by stress fiber reorientation and self-adjustment of their reference length. At high frequency (>1 Hz), the only way stress fibers can minimize the perturbation in fiber stretch is by alignment perpendicular to the direction of stretch. At lower frequencies, fiber self-adjustment becomes important.

There are two characteristic times describing the stress fiber response to cyclic stretch. One characteristic time is the time constant for stress fiber self-adjustment (τ) determining the sensitivity of stress fiber to the frequency of stretch, while the other is that for stress fiber disassembly ($\frac{1}{k^i}$) which depends on the level of perturbation of fiber stretch from the set-point level. When the characteristic time constant τ is shorter than the period of a cycle of stretch, the stress fibers can respond quickly enough to self-equilibrate to maintain stress fiber stretch at the set-point level. In contrast, the amplitude of stress fiber extension follows that of the normal matrix strain when the characteristic time constant τ is much greater than the period of the stretch cycle. Next consider the time constant for fiber turnover. For cyclic uniaxial stretch, the time constant for stress fiber disassembly in the perpendicular direction of matrix stretch is much greater than that in the parallel direction, leading to the accumulation of stress fibers in the perpendicular direction. The asymmetry in the time constant for stress fiber disassembly decreases at low stretch frequencies (<0.1 Hz) since stress fiber self-adjustment reduces the perturbation in stress fiber extension from the set-point level. Consequently, the extent of stress fiber alignment (i.e., the steady-state value for circular variance) is

proportional to stretch frequency since the rate of stretching is faster than the rate of stress fiber self-adjustment.

Due to the role of stress fiber self-adjustment, this mathematical model predicts that there is a threshold frequency of ~0.01 Hz, below which stress fibers are able to self-adjust in order to maintain stress fiber stretch at the set-point value. As the frequency of stretch increases from 0.01 to 1 Hz, the cells become increasingly less capable of adjusting to matrix stretch-induced changes in stress fiber stretch. On the other hand, in order to compensate for the change, stress fibers become oriented toward the direction of lowest perturbation in stretch based on the mechanism of stress fiber turnover (i.e., perpendicular to the direction of stretch). The stochastic model also predicts that there is an upper threshold frequency of ~1 Hz stretch where near-maximal stress fiber alignment occurs. The model predicts that increasing the stretch above 1 Hz would not lead to any additional alignment of the stress fiber. Our stretch device is unable to generate stretch above 1 Hz; however, Jungbauer and colleagues (2008) applied frequencies ranging from 0.0001 to 20 Hz and reported a threshold frequency of 1 Hz.

The stochastic model of stress fiber reorientation in response to cyclic matrix stretch shares some key features of a recent model proposed by De et al. (2007). In their deterministic model, cells subjected to stretch readjust their contractile activity in an attempt to maintain either the local stress or strain in the surrounding matrix at a set-point value while being subjected to a periodic external stress (De et al., 2008). At low frequencies of cyclic stress, the cells are able to readjust their contractile activity so as to maintain the mechanical state of the matrix at the set-point value and the cells orient parallel to the direction of stress. In contrast, at high frequencies the cells orient nearly

perpendicular to the applied stress since the changes in contractile activity are too slow to compensate. In our stochastic model in which a periodic stretch is applied, stress fibers attempt to maintain constant the level of strain in the stress fibers, not in the surrounding matrix. At low stretch frequencies, the stress fibers are able to readjust their extension so as to maintain stretch at the set-point level with the result that the stress fibers do not orient in any direction. The contrasting results at low frequencies are attributable to the difference in the boundary conditions – De et al. (2007) use traction boundary conditions, while the present model uses displacement boundary conditions. When the displacement is sufficiently slow, the cells essentially no longer sense the changing boundary conditions, while a cell would be expected to continue to sense a static or quasi-static stress. In the case of cells subjected to cyclic stretch on elastomeric substrates such as silicone rubber, the displacement boundary condition is a more appropriate description of the mechanical stimulus that the cells respond to. This is consistent with the concept of ‘‘stress shielding’’ in which stress in tissues is primarily borne by the matrix and is not transmitted to the resident cells (Wang et al., 2001). Traction boundary conditions are expected to be more important in matrices with relatively low elastic moduli such as collagen hydrogels (Brown et al., 1998). Wei et al. (2008) proposed a dynamic model of cyclic stretch-induced stress fiber orientation in which stress fiber growth depends on the rate of stress fiber shortening. They also predict that stress fiber alignment depends on stretch magnitude and frequency, although the extent of alignment does not have a threshold at 0.01 Hz and does not saturate at 1 Hz.

Parameter sensitivity analysis illustrates the effect of each model parameter on the system response. The rate and extent of stress fiber alignment are primarily dependent on

the values of k_0 and k_1, respectively, which is similar to deterministic model (cf. Section II.C.3). The third model parameter,τ, primarily determines the frequency range over which circular variance transitions between the maximum and minimum values (i.e., the threshold and saturation values). In the literature survey, only a few studies report the effects of frequency on stress fiber alignment. Liu et al. (2008) investigated the potential role of the cyclic strain frequency ranging from 0.5 to 2 Hz in vitro showing that cyclic strain at 0.5 Hz was the most effective frequency influencing the alignment of aortic smooth muscle cell. Wider range of stretch frequencies from 0.0001 to 20 Hz was tested by Jungbauer et al. who concluded that stretch frequency plays an important role in both the rate and extent of fibroblast alignment. Jungbauer and colleagues also reported a saturation frequency of 1 Hz for stretch-induced cell alignment, which is consistent with the predictions of our stochastic model. In contrast, Wille et al. (2004) concluded there was no dependence on the rate of stretching on the orientation of non-confluent human aortic endothelial cells in response to pure uniaxial cyclic stretching; however, their experiments were limited to a range between 0.5 to 1 Hz which may not be sufficient to detect an effect of frequency. This stochastic model estimated a time constant for fiber self-adjustment of 0.5 *s* to describe the measured transition of stress fiber alignment from essentially no alignment at 0.01 Hz to extensive alignment at 1 Hz. The time constant of 0.5 *s* is shorter than the value of ~6 *s* obtained by Kumar et al. (2006) from measured retraction rates of severed stress fibers in bovine capillary ECs. It is possible that self-adjustment occurs at different rates depending on if the stress fiber is lengthening or shortening, in which case the value of 0.5 *s* from the current study would represent an average of the two time constants. Another potential explanation is that cells from

different vascular beds have different rates of self-adjustment. Arterial ECs are subjected to high frequency stretch (~1 Hz), hence may need to be more responsive to time-changing strains than capillary ECs that experience much less frequent changes in matrix strain. The phenomenological description of the self-adjustment of stress fiber mechanical equilibrium needs to be supported with more mechanistic details, such as the kinetics of actin-myosin cross bridging and α-actinin binding (Hotulainen and Lappalainen, 2006).

In summary, the stochastic model is able to describe the frequency-dependent of stress fiber alignment by incorporating expressions describing the turnover and self-adjustment of stress fibers. The results indicate that stress fiber self-adjustment determines the frequency dependency, while stress fiber turnover determines the maximum extent of the stress fiber orientation possible at high stretch frequencies. Importantly, these results indicate that stress fiber self-adjustment provides cells a fading memory of the deformations of the tissues they reside upon.

IV. GENERAL DISCUSSION AND CONCLUSIONS

The modeling studies were very successful in describing the general dynamics of stress fiber reorganization in response to cyclic matrix stretching. For stretch at relatively high frequencies (i.e., 1 Hz), the models are able to describe the gradual redistribution of stress fiber orientations in experimental data including the magnitude-dependent alignment of stress fibers perpendicular to the direction of cyclic uniaxial, the lack of stress fiber alignment induced by cyclic equibiaxial stretch, and the change in stress fiber orientation in response to a change in the direction of cyclic uniaxial stretch. In order to describe the frequency-dependence of stretch-induced alignment, we included time-dependent material properties to the stress fibers into a stochastic version of the model. Thus, we have developed, for the first time, a generalized model to describe the response of stress fibers to various spatially and temporally changing stretch patterns. With such a quantitative model, we hope to more clearly understand how cells are able sense their mechanical environment and tailor their response.

Models are only useful to describe particular phenomena when the assumptions used are applicable, thus the basic assumptions used to formulate the models must be considered critically. It has been reported that the deformation of the body of ECs closely follows that of the substrate (Caille et al., 1998). Ventral stress fibers, being firmly adhered to the substrate at both ends via focal adhesions, are likely to follow the substrate very closely. Therefore, it is suitable that the affine strain approximation (cf. Eq. (1)) was employed to calculate the contribution of matrix stretch to the stretch of individual stress fibers. Stress fibers have a much higher tensile stiffness than bending stiffness (Deguchi et al., 2005c). Consequently, higher stress is developed in response to stretching a stress

fiber along it axis than in the transverse direction, implying that normal fiber stretch is the predominant strain transmitted to stress fibers (cf. Section II.B.1.d). Another important consideration is the assumptions that stress fibers are constrained to move together (cf. Section II.B.1.c), but each stress fiber assembles and disassembles independently of the others (cf. Section II.B.1.e). Kumar et al. (2006) demonstrated that cutting individual stress fibers with laser scissors did not cause adjacent stress fibers to remodel or change their arrangements. This observation suggests that the assembly or disassembly of individual stress fibers may not significantly change the stretch experienced by neighboring stress fibers. The presumed existence of an equilibrium fiber prestretch is supported by experiments demonstrating that there is little variance in fiber prestretch between stress fibers within individual ECs and between different ECs (Lu et al., 2008). Further, even if a perturbation stretch in matrix may change fiber prestretch, the same level of fiber prestretch is still achieved hours later. Katoh et al. (2001) reported the existence of two separate types of stress fibers, central and peripheral fibers, that differ in their contraction rate, thickness, and location in the cell. Also, Deguchi et al. (2005c) demonstrated that tension in stress fibers are transmitted to other stress fibers that linked to them. Thus, the assumption that all stress fibers response to matrix stretch independently and in a similar manner is oversimplified and should be addressed in subsequent models.

The assumption that total mass fraction of actin stress fibers contained in the cell is constant over time is also an oversimplification. Actin constantly depolymerizes into monomers (G-actin) and polymerizes into filamentous polymers (F-actin). Further, F-actin exists as both a loose network of narrow filaments and bundled filaments that make

up stress fibers. Stress fibers have been shown to initially disassemble and gradually reassemble in response to matrix stretch (Lu et al., 2008). Pender and McCulloch (1991) reported that total F-actin content can change quickly immediately after matrix stretching. Since the current models only deal with population dynamics of stress fibers, the models should be refined in the future to include additional populations of actin and incorporate appropriate kinetics for the exchange of actin between these populations. Further, adherent animal cells contain at least three categories of stress fibers: ventral stress fibers, transverse arcs, and dorsal stress fibers (Hotulainen and Lappalainen, 2006). Since only ventral stress fibers are associated at both ends to focal adhesions, the stress fibers our models are only meant to describe ventral stress fibers. Based on the observation that the stress fibers in BAECs cultured on the stretch chambers are associated with focal adhesions at each end, it is likely that ventral stress fibers are the dominant category of stress fibers in these cells. Transverse arcs and dorsal stress fibers are expected to appear transiently during the formation of ventral stress fibers and disappear when they are converted to ventral stress fibers (Hotulainen and Lappalainen, 2006); however, the present models do not address their roles in the formation of stress fibers.

The current models are limited to describing a population of stress fibers and do not consider other factors that may interact with stress fibers during stretch-induced reorientation. For example, cell elongation and stress fiber orientation are generally tightly coupled in highly polarized cells such as fibroblasts and smooth muscle cells, and less so in more highly spread cells such as endothelial cells. Stress fiber assembly and reorientation has been reported to drive endothelial cell elongation (Noria et al., 2004). In contrast, Civelekoglu et al. (2005) proposed that endothelial cell elongation drives the

orientation of stress fibers. In our models, the assumption that new fibers are allowed to assemble in any direction with equal probability is an oversimplification; it is likely that fiber assembly depends on cell shape, as well as the predominant orientations of the existing stress fiber population. These factors are expected to provide an initial virtual inertia for stretch-induced stress fiber reorientation, which may contribute to the ~15 minute delay before the circular variance in stress fiber orientation began to decrease at a rate similar to that predicted for cyclic stretch at 1 Hz (cf. Fig. 16). Further, it has been reported that stress fibers are transiently disrupted immediately after initiating cyclic stretch and reassemble over a course of minutes to hours (Hayakawa et al., 2001; Wille etal.,2004). Such transient disruption of stress fibers indicates that the rate of fiber assembly initially lags behind the rate of fiber disassembly since stress fiber assembly is a gradual process that involves actin polymerization and bundling, as well as focal adhesion assembly. The rates of these processes are expected to also influence the rate of stress fiber alignment. In future refinements of the current models, we will investigate the relationships amongst stretch-induced changes in cell shape, stress fiber and focal adhesion formation, and stress fiber reorientation to identify an appropriate expression for the rate of fiber assembly. Although stress fiber remodeling is a complex process involving more than simple disappearance and reappearance of stress fibers within a cell, it is noteworthy that a simple model describing stress fiber disassembly and reassembly with just two parameters (k_0 and k_1) was capable of accurately describing the temporal and spatial reorganization of stress fibers in both uniaxial and equibiaxial cyclic stretches.

The simulation results of the deterministic model predict that stress fiber alignment in response to cyclic uniaxial stretch reduces the perturbation in fiber stretch as well as the

rate of fiber turnover, while both of these parameters remain elevated in response to cyclic equibiaxial stretch (cf. Fig. 11). The alignment of stress fibers is a gradual process that occurs over a period of hours, and the time course of stress fiber alignment correlates with the activation pattern of stretch-induced signal transduction (Kaunas et al., 2006; Naruse et al.,1998a, b). Based on the role of stress fibers in regulating both cell structure and mechanotransduction, we expect the model will provide insight into the effects of different patterns of stretch on cell signaling. For example, cyclic uniaxial and equibiaxial stretches result in transient and sustained activation of JNK, respectively (Kaunas et al., 2006). The mitogen-activated protein kinases JNK can regulate AP-1 transcription factor which mediates the expression of several genes induced by mechanical stimuli, including endothelin-1 (Wang et al., 1993), intercellular adhesion molecule-1 (ICAM-1) (Cheng et al., 1996) and monocyte chemoattractant protein-1 (MCP-1) (Wang et al., 1995), which are involved in the early stages of atherosclerosis (Clinton et al., 1992, Davies et al, 1993, and Lerman et al., 1993). Katsumi et al. (2005) reported that JNK activation in response to stretch requires formation of new integrin attachments. This result suggests that the rate of focal adhesion turnover regulates JNK activation since ventral stress fiber assembly requires the formation of integrin bonds at the associated focal adhesions. Stretch has also been reported to induce conformational changes in the cytoskeleton and/or associated focal adhesions that contribute to signal transduction (Sawada and Sheetz, 2002; Cunningham et al., 2002). JNK activation, therefore, appears to occur under conditions of high amplitudes in fiber stretch and/or high rates of fiber turnover. According to the mathematical models, perturbing fiber stretch from the homeostatic level greatly accelerates stress fiber turnover and increases the level of fiber stretch. A

sustained increase in the turnover of stress fibers and/or the amplitude of fiber stretch may result in chronic activation of JNK (i.e., in the case of cyclic equibiaxial stretch), while a transient increase in the turnover and/or the amplitude of fiber stretch as the stress fibers align perpendicular to stretch, may lead to transient activation of JNK (i.e., in the case of cyclic uniaxial stretch). Further, the simulation results of the stochastic model predicted the frequency-dependent of stress fiber turnover rates, as well as fiber stretch amplitude, in response to both cyclic uniaxial and equibiaxial stretch (cf. Fig. 17A-B and Fig. 18B-C). Therefore, the model predicts that stretch-induced JNK activation is also dependent on the frequency of stretch; however, this remains to be demonstrated experimentally. Thus, these studies may serve as the framework to build a model coupling cytoskeletal dynamics with JNK activation to predict distinct temporal patterns of JNK activation in response to different spatiotemporal patterns of matrix stretch.

McGrath et al. (2000) have reported that actin filament turnover is faster in non-confluent ECs than confluent cells, which is consistent with our results (cf. Figs. 7 and 16). Since the stochastic model describes the experiment data of non-confluent ECs while the deterministic model fits to that of confluent ECs, the rate of stress fibers alignment in stochastic model is faster than that in deterministic model. Thus the value of α_0 is higher in stochastic model than that in deterministic model (3×10^{-4} vs. $10^{-6}\, s^{-1}$). In addition, the extent of alignment in stochastic model (cf. Fig. 16) is somewhat less than that for confluent ECs (cf. Fig. 7). This behavior may be attributed to the contribution of cell-cell junctions, which may act to reinforce mutual alignment of neighboring cells and their stress fibers when cells are confluent. Indeed, in static cell culture, localized co-alignment of stress fibers are typically observed in small groups of

cells. When subjected to cyclic uniaxial stretch, all cells tend to align perpendicular to the direction of stretch and the localized reinforcement may augment the uniformity of the stress fiber alignment under confluent conditions.

In summary, while the results of the present models are promising, there is clearly room for improvement. Thus, the research reported in this thesis provides guidance toward the development of more realistic mathematical descriptions of stress fiber remodeling. The mathematical models of stress fiber networks can be applied to stretch-induced stress fiber remodeling and predict the cell signaling in many cell types subjected to any two-dimensional matrix stretch pattern. It is worth noting that the mathematical models have predictive capability and suggest experiments that will provide increased mechanistic insight and thus facilitate refinement of the models. While these simple models describe general characteristics of stretch-induced stress fiber dynamics, they cannot completely describe the complex reorganization of actin filaments within individual cells. In future, more sophisticated models will be developed based on the current models.

REFERENCES

Baek, S., K. R. Rajagopal, and J. D. Humphrey, (2005). Competition between radial expansion and thickening in the enlargement of an intracranial saccular Aneurysm. *J. of Elasticity* **80**: 13-31.

Balaban, N. Q., U. S. Schwarz, D. Riveline, P. Goichberg, G. Tzur, I. Sabanay, D. Mahalu, S. Safran, A. Bershadsky, L. Addadi, and B. Geiger, (2001). Force and focal adhesion assembly: a close relationship studied using elastic micropatterned substrates. *Nat. Cell Biol.* **3**: 466-472.

Brown, R. A., R. Prajapati, D. A. McGrouther, I. V. Yannas, and M. Eastwood, (1998). Tensional homeostasis in dermal fibroblasts: mechanical responses to mechanical loading in three-dimensional substrates. *J. Cell Physiol.* **175**: 323-332.

Burridge, K., K. Fath, T. Kelly, G. Nuckolls, and C. Turner, (1988). FOCAL ADHESIONS: Transmembrane junctions between the extracellular matrix and the cytoskeleton. *Ann. Rev. Cell Biol.* **4**: 487-525.

Caille, N., Y. Tardy, and J. J. Meister, (1998). Assessment of strain field in endothelial cells subjected to uniaxial deformation of their substrate. *Ann. Biomed. Eng.* **26**: 409-416.

Canadas, P., V. M. Laurent, C. Oddou, D. Isabey, and S. Wendling, (2002). A cellular tensegrity model to analyse the structural viscoelasticity of the cytoskeleton. *J. Theor. Biol.* **218**: 155-173.

Chen, C. S., J. Tan, and J. Tien, (2004). Mechanotransduction at cell-matrix and cell-cell contacts. *Ann. Rev. Biomed. Eng.* **6**: 275-302.

Cheng, J. J., B. S. Wung, Y. J. Chao, and D. L. Wang, (1996). Cyclic strain enhances adhesion of monocytes to endothelial cells by increasing intercellular adhesion molecule-1 expression. *Hypertension* **28** (3): 386-391.

Chien, S., (2007). Mechanotransduction and endothelial cell homeostasis: the wisdom of the cell. *Am. J. Physiol. Heart Circ. Physiol.* **292**:1209-1224.

Chien, S., (2008). Effects of disturbed flow on endothelial cells. *Ann. of Biomed. Eng.* **36**(4): 554-562.

Civelekoglu-Scholey G., A. W. Orr, I. Novak, J.-J. Meister, M. A. Schwartz, and A. Mogilner, (2005). Model of coupled transient changes of Rac, Rho, adhesions and stress fibers alignment in endothelial cells responding to shear stress. *J. Theor. Biol.* **232**: 569-585.

Clinton, S. K., R. Underwood, L. Hayes, M. L. Sherman, D. W. Kufe, and P. Libby, (1992). Macrophage colony-stimulating factor gene expression in vascular cells and in experimental and human atherosclerosis. *Am. J. Pathol.* **140** (2): 301-316.

Cunningham, J. J., J. J. Linderman, and D. J. Mooney, (2002). Externally applied cyclic strain regulates localization of focal contact components in cultured smooth muscle cells. *Ann. Biomed. Eng.* **30**: 927-935.

Davies, M. J., J. L. Gordon, A. J. Gearing, R. Pigott, N. Woolf, D. Katz, and A. Kyriakopoulos, (1993). The expression of the adhesion molecules ICAM-1, VCAM-1, PECAM, and E-selectin in human atherosclerosis. *J. Pathol.* **171** (3): 223-229.

De, R., A. Zemel, and S. A. Safran, (2007). Dynamics of cell orientation. *Nature Physics* **3**: 655-659.

Deguchi, S., T. Ohashi, and M. Sato, (2005a). Evaluation of tension in actin bundle of endothelial cells based on preexisting strain and tensile properties measurements. *Mol. Cell Biomech.* **2**: 125-133.

Deguchi, S., T. Ohashi, and M. Sato, (2005b). Tensile properties of single stress fibers isolated from cultured vascular smooth muscle cells. *J. of Biomech.* **39**: 2603-2610.

Deguchi, S., T. Ohashi, and M. Sato, (2005c). Intracellular stress transmission through actin stress fiber network in adherent vascular cells. *Mol. Cell Biomech.* **2**: 205–216.

Evans, E. A. and D. A. Calderwood, (2007). Forces and bond dynamics in cell adhesion. *Science* **316**: 1148-1153.

Frangos, S. G., V. Gahtan, and B. Sumpio, (1999). Localization of atherosclerosis: Role of hemodynamics. *Arch. Surg.* **134**: 1142-1149.

Fung, Y.C., (1994). A first course in contiuum mechanics. Prentice-Hall Inc., Englewood Cliffs, NJ.

Gimbrone, M. A., Jr., (1999). Vascular endothelium, hemodynamic forces, and atherogenesis. *Am. J. of Pathol.* **155**: 1-5.

Gimbrone, M. A., Jr., (1999). Endothelial dysfunction, hemodynamic forces, and atherosclerosis. *Thromb. haemost.* **82**(2): 722-726.

Gleason, R. L. and J. D. Humphrey, (2004). A mixture model of arterial growth and remodeling in hypertension: altered muscle tone and tissue turnover. *J. Vasc. Res.* **41**: 352-363.

Hahn, C. and M. A. Schwartz, (2008). The role of cellular adaptation to mechanical forces in atherosclerosis. *Arterioscle. Thromb. Vasc. Biol.* **28**: 2101-2107.

Hayakawa, K., N. Sato, and T. Obinata, (2001). Dynamic reorientation of cultured cells and stress fibers under mechanical stress from periodic stretching. *Exp. Cell Res.* **268**: 104-114.

Hotulainen, P., and P. Lappalainen, (2006). Stress fibers are generated by two distinct actin assembly mechanisms in motile cells. *J. Cell Biol.* **173**: 383-394.

Hsu, H.-J., C.-F. Lee, and R. Kaunas, (2009). A dynamic stochastic model of frequency-dependent stress fiber alignment induced by cyclic stretch. *PLoS ONE* **4**(3): e4853.

Humphrey, J. D. and K. R. Rajagopal, (2003). A constrained mixture model for arterial adaptations to a sustained step change in blood flow. *Biomech. Model Mechanobiol.* **2**: 109-126.

Jungbauer, S., H. Gao, J. P. Spatz, and R. Kemkemer, (2008). Two characteristic regimes in frequency dependent dynamic reorientation of fibroblasts on cyclically stretched substrates. *Biophys. J.* **95**: 3470-3478.

Katoh, K., Y. Kano, M. Amano, K. Kaibuchi, and K. Fujiwara, (2001). Stress fiber organization regulated by MLCK and Rho-kinase in cultured human fibroblasts. *Am. J. Physiol. Cell Physiol.* **280**: C1669-C1679.

Katsumi, A., T. Naoe, T. Matsushita, K. Kaibuchi, and M. A. Schwartz, (2005). Integrin activation and matrix binding mediate cellular responses to mechanical stretch. *J. Biol. Chem.* **280**: 16546-16549.

Kaunas, R., P. Nguyen, S. Usami, and S. Chien, (2005). Cooperative effects of Rho and mechanical stretch on stress fiber organization. *Proc. Natl. Acad. Sci. U S A* **102**(44): 15895-15900

Kaunas, R., S. Usami, and S. Chien, (2006). Regulation of stretch-induced JNK activation by stress fiber orientation. *Cellular Signaling* **18**: 1924-1931.

Kaunas, R. and H.-J. Hsu, (2009). A kinematic model of stretch-induced stress fiber turnover and reorientation. *J. of Theor. Biol.* **257**(2): 320-333.

Kumar, S., I. Z. Maxwell, A. Heisterkamp, T. R. Polte, T. P. Lele, M. Salanga, E. Mazur, and D. E. Ingber, (2006). Viscoelastic retraction of single living stress fibers and its impact on cell shape, cytoskeletal organization, and extracellular matrix mechanics. *Biophys. J.* **90**: 3762-3773.

Lerman, A., M. W. Webster, J. H. Chesebro, W. D. Edwards, C. M. Wei, and V. Fuster, J. C. Burnett, Jr., (1993). Circulating and tissue endothelin immunoreactivity in hypercholesterolemic pigs. *Circulation* **88** (6): 2923-2928.

Liu, B., M. J. Qu, K. R. Qin, H. Li, and Z. K. Li, (2008). Role of cyclic strain frequency in regulating the alignment of vascular smooth muscle cells in vitro. *Biophys. J.* **94**: 1497-1507.

Lu, L., Y. Feng, W. J. Hucker, S. J. Oswald, G. D. Longmore, and F. C. Yin, (2008). Actin stress fiber pre-extension in human aortic endothelial cells. *Cell Motil. Cytoskeleton* **65**: 281-294.

Magdalena, C.-W. and K. Burridge, (1996). Rho-stimulated contractility drives the formation of stress fibers and focal adhesions. *J. of Cell Biol.*, **133**(6): 1403-1415.

McGrath, J. L., E. A. Osborn, Y. S. Tardy, C. F. Dewey, Jr., and J. H. Hartwig, (2000). Regulation of the actin cycle in vivo by actin filament severing. *Proc. Natl. Acad. Sci. U S A* **97**: 6532-6537.

Na, S., G. A. Meininger, and J. D. Humphrey, (2007). A theoretical model for F-actin remodeling in vascular smooth muscle cells subjected to cyclic stretch. *J. of Theor. Biol.* **246**: 87-99.

Naruse, K., T. Yamada, and M. Sokabe, (1998a). Involvement of SA channels in orienting response of cultured endothelial cells to cyclic stretch. *Am. J. Physiol.* **274**: H1532-H1538.

Naruse, K., X. Sai, N. Yokoyama, and M. Sokabe, (1998b). Uni-axial cyclic stretch induces c-src activation and translocation in human endothelial cells via SA channel activation. *FEBS Lett.* **44**1: 111-115.

Nerem, R. M., (1993). Hemodynamics and the vascular endothelium. *Biomech. Eng.* **115**: 510-514.

Noria, S., F. Xu, S. McCue, M. Jones, A. I. Gotlieb, et al., (2004). Assembly and reorientation of stress fibers drives morphological changes to endothelial cells exposed to shear stress. *Am. J. Pathol.* **164**: 1211-1223.

Pelham, R. J., Jr. and Y.-L. Wang, (1997). Cell locomotion and focal adhesions are regulated by substrate flexibility. *Proc. Natl. Acad. Sci.* **94**: 13661-13665.

Pender N. and C. A. McCulloch, (1991). Quantitation of actin polymerization in two human fibroblast sub-types responding to mechanical stretching. *J. of Cell. Science.* **100**: 187-193.

Polte T. R., G. S. Eichler, N. Wang, and D. E. Ingber, (2004). Extracellular matrix controls myosin light chain phosphorylation and cell contractility through modulaiton of cell shape and cytoskeletal prestress. *Am. J. Physiol.* **286**:C518–C528.

Sawada, Y. and M. P. Sheetz, (2002). Force transduction by Triton cytoskeletons. *J. Cell Biol.* **156**: 609-615.

Takemasa, T., K. Sugimoto, and K. Yamashita, (1997). Amplitude-dependent stress fiber reorientation in early response to cyclic strain. *Exp. Cell Res.* **230**:407-410.

Takemasa T., T. Yamaguchi, Y. Yamamoto, K. Sugimoto, and K. Yamashita, (1998). Oblique alignment of stress fibers in cells reduces the mechanical stress in cyclically deforming fields. *Eur. J. Cell Biol.* **77**: 91-99.

Wang, D. L., C. C. Tang, B. S. Wung, H. H. Chen, M. S. Hung, and J. J. Wang, (1993). Cyclical strain increases endothelin-1 secretion and gene expression in humanendothelial cells. *Biochem. Biophys. Res. Commun.* **195**(2): 1050-1056.

Wang, D. L., B. S. Wung, Y. J. Shyy, C. F. Lin, Y. J. Chao, S. Usami, and S. Chien, (1995). Mechanical strain Induces monocyte chemotactic protein-1 gene expression in

endothelial cells: Effects of mechanical strain on monocyte adhesion to endothelial cells. *Circ. Res.* **77**(2): 294-302.

Wang, J. H.-C, (2000). Substrate deformation determines actin cytoskeleton reorganization: A mathematical modeling and experimental study. *J. theor. Biol.* **202**: 33-41.

Wang, J. H.-C., G.-C. Pascal, and C.-P. F. Yin, (2000). Contractility affects stress fiber remodeling and reorientation of endothelial cells subjected to cyclic mechanical stretching. *Annals. of Biomed. Eng.* **28**: 1165-1171.

Wang, J. H.-C., G.-C. Pascal, W. Jeremiah, and C.-P. F. Yin, (2001). Specificity of endothelial cell reorientation in response to cyclicmechanical stretching. *J. of Biomech.* **34**: 1563-1572.

Wei Z., V. S. Deshpande, R. M. McMeeking, and A. G. Evans, (2008). Analysis and interpretation of stress fiber organization in cells subject to cyclic stretch. *J. Biomech. Eng.* **130**: 031009.

Wille J. J., C. M. Ambrosi, and F. C. Yin, (2004). Comparison of the effects of cyclic stretching and compression on endothelial cell morphological responses. *J. Biomech. Eng.* **126**: 545-551.

Yamada, H., T. Takemasa, and T. Yamaguchi, (2000). Theoretical study of intracellular stress fiber orientation under cyclic deformation. *J. of Biomech.* **33**: 1501-1505.

Yoshigi, M., E. B. Clark, and H. J. Yost, (2003). Quantification of stretch-induced cytoskeletal remodeling in vascular endothelial cells by image processing. *Cytometry* **55**(A): 109-118.

APPENDIX A. FIGURES

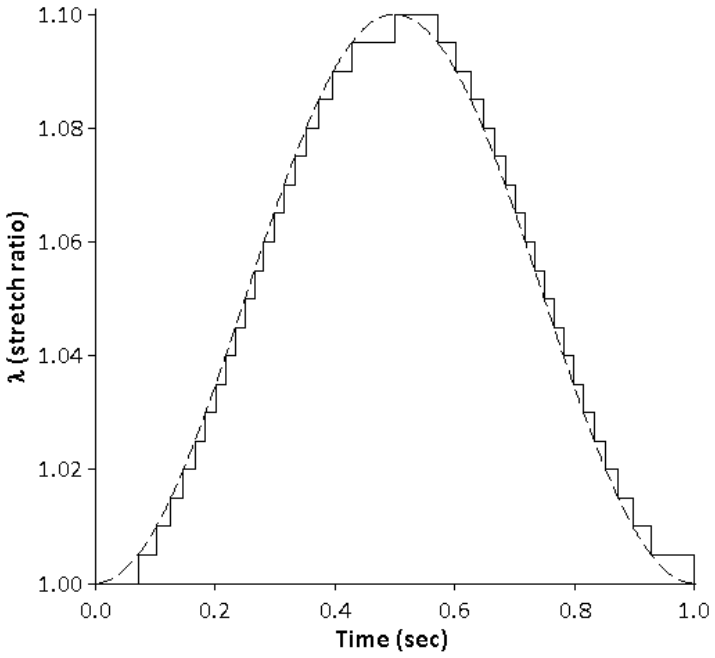

Fig. 1. Simulated sinusoidal stretch pattern. One cycle of simulated 10% cyclic sinusoidal matrix stretch at 1 Hz (solid lines) are shown with consisting of 20 steps of magnitude $\lambda = 1.1^{0.05}$ during the first half-cycle and 20 steps of magnitude $\lambda = 1.1^{0.05}$ during the second half of the cycle. The duration of each step was varied to simulate a sinusoidal function.

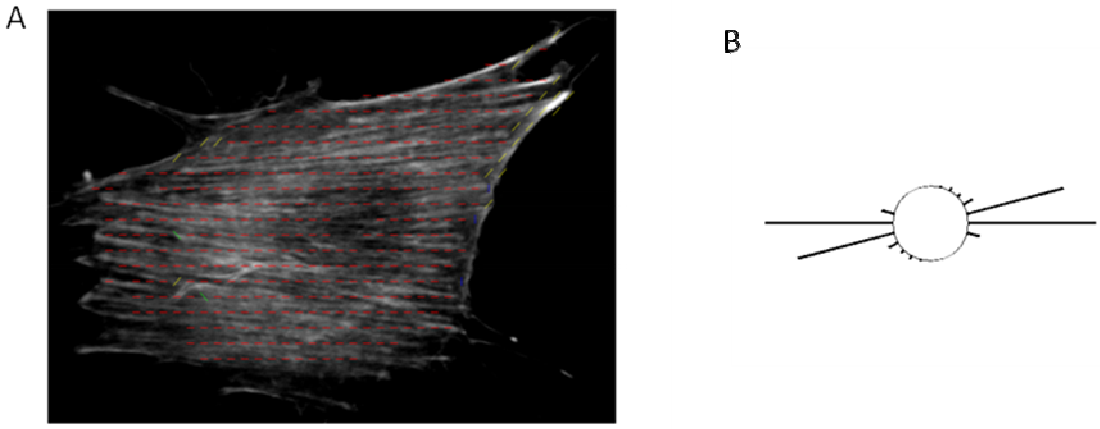

Fig. 2. Computed the extent and histogram of stress fiber orientation. (A) Representative the image of a single BAECs subjected to 6 hr of cyclic stretch (10% linear strain) at frequency of 1 Hz. The cell was fixed and stained for the boundary and stress fibers (while lines) following the stretch experiment. The orientations of stress fibers were computed and plotted (red lines). The extent of stress fiber alignment was computed as 0.09. **(B)** The circular histogram was plotted for the distribution of stress fibers.

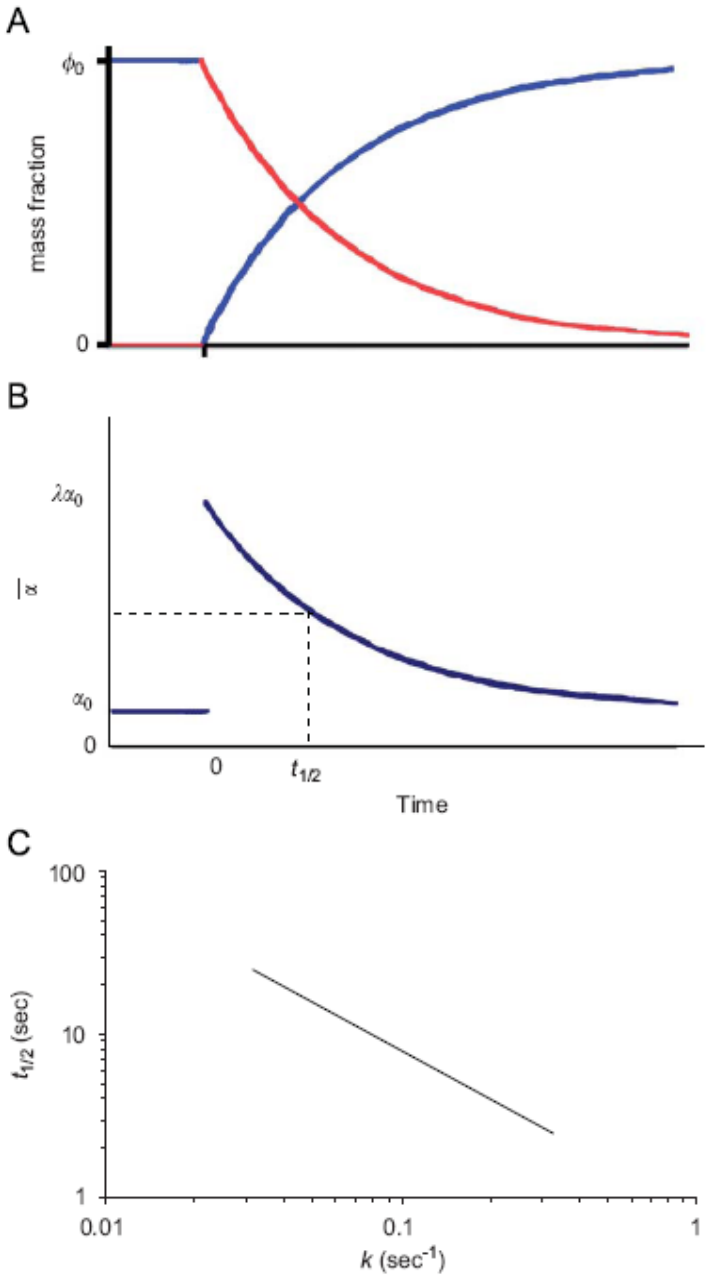

Fig. 3. Response to a step-change in equibiaxial stretch of magnitude λ: (A) Before substrate stretching, all the fibers have a basal level of stretch α_0. Immediately after substrate stretching, all the fibers have a stretch of $\lambda\alpha_0$, and then these fibers are replaced overtime with fibers with a basal stretch α_0. **(B)** Plot of average fiber stretch ($\bar{\alpha}$) overtime. Initially, the fiber stretch is α_0 for all fibers, and then the mass-average fiber stretch $\bar{\alpha} = \phi_0\alpha_0 + \phi_1\lambda\alpha_0$ returns to α_0 as the old fibers are replaced by new fibers with $\bar{\alpha} = \alpha_0$. The half-life ($t_{1/2}$) of the decrease in fiber stretch is indicated by dashed lines. **(C)** The relationship between the rate constant and the half-life is shown as a function of the rate constant k.

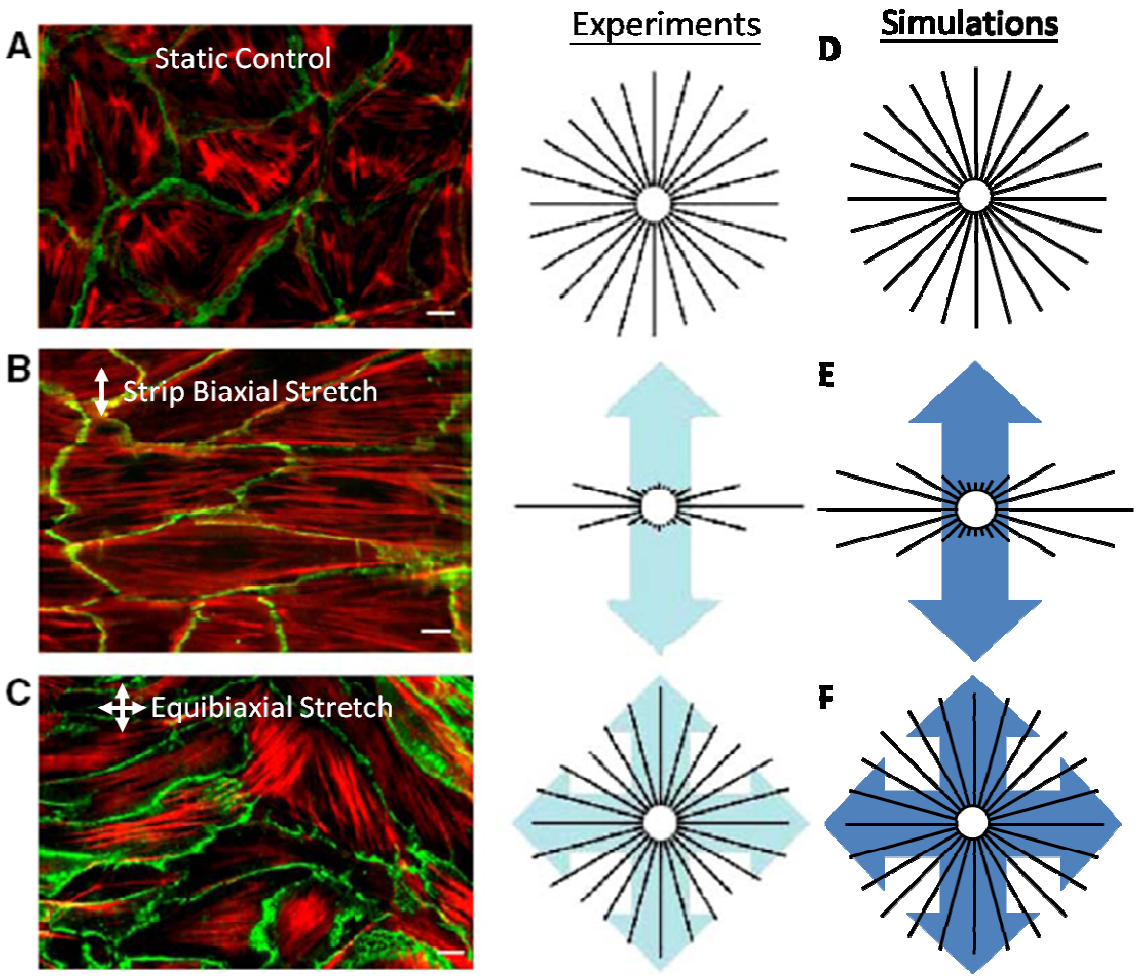

Fig. 4. Comparison of experimentally measured and simulated stress fiber distributions. (A-C) Representative images of confluent BAECs either kept as static controls (A) or subjected to 6 hr of 1.1 stretch ratio, 1 Hz cyclic uniaxial (B) or equibiaxial (C) stretch, fixed, and stained for F-actin (from Kaunas et al., 2006). The distributions of stress fiber orientations were determined using an intensity gradient algorithm and the results from multiple cells (n=50 cells) are summarized as angular histograms (direction of stretch is shown in blue). **(D-F)** Circular histograms of simulations of static controls (D), or 6 hr of 1.10 stretch ratio, 1 Hz cyclic uniaxial (E) and equibiaxial stretch (F) for $k_0 = 10^{-6}\ s^{-1}\ and\ k_1 = 2.5 \times 10^5\ s^{-1}$

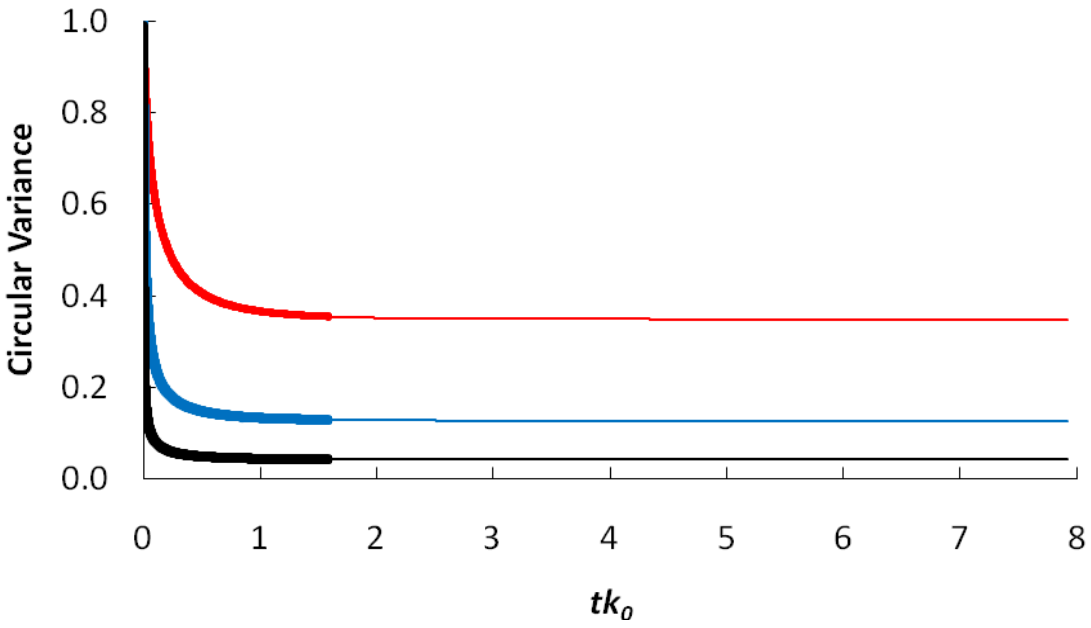

Fig. 5. The rate constants k_0 and k_1 determine the rate and extent of stress fiber alignment. Simulations of sinusoidal cyclic uniaxial stretch of amplitude 1.10 and frequency 1 Hz were performed over a range of values for k_0 values of 10^{-4} (thin curves) and 10^{-5} (thick curves), and k_1 values of 10^3 (red curves), 10^4 (blue curves), and 10^5 (black curves). Circular variance was plotted versus non-dimensionalized time tk_0 to illustrate that the rate of alignment scales with k_0, while the steady-state response depends on k_1.

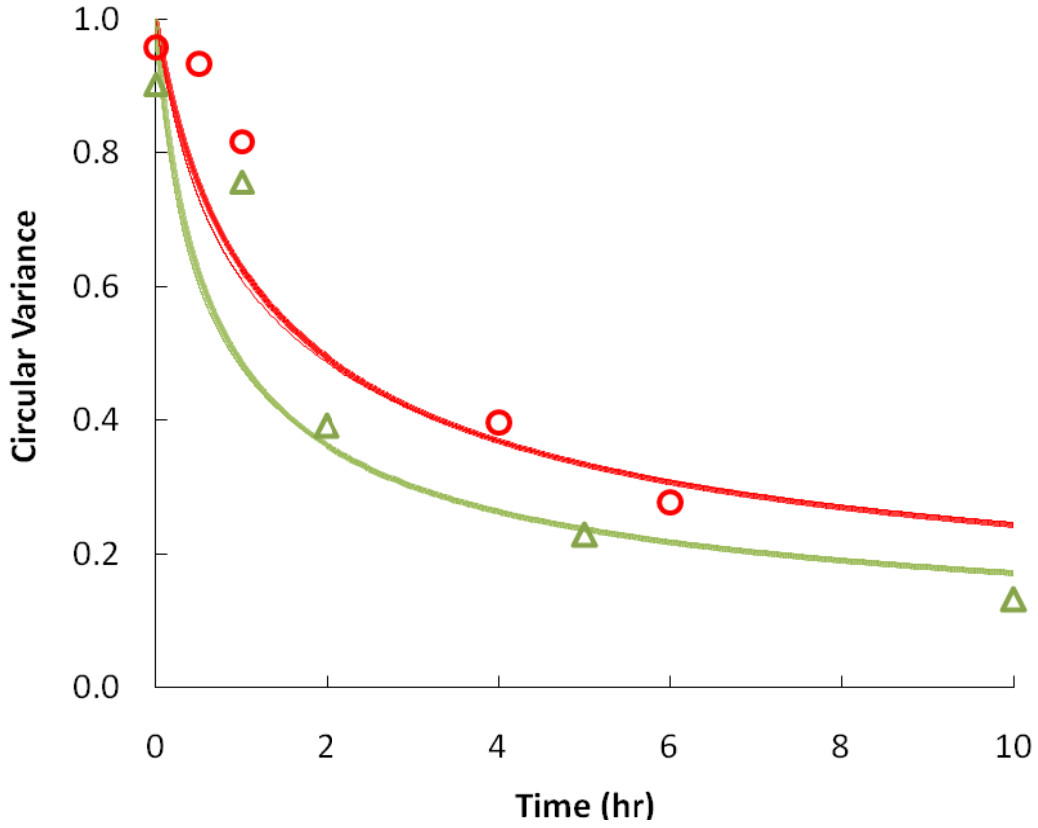

Fig. 6. Comparison of nonlinear and linear relationship between k^i and α^i. Simulations of sinusoidal cyclic uniaxial stretch of amplitude 1.10 were performed using the linear relationship between k^i and α^i fitting the data for Kaunas et al. (red circles) and Yoshigi et al. (green triangles) with the rate parameters $k_0 = 10^{-6}\ s^{-1}$ and $k_1 = 1.6 \times 10^4\ s^{-1}$ (dash, red line) and $k_0 = 10^{-6}\ s^{-1}$ and $k_1 = 3.3 \times 10^4\ s^{-1}$ (dash, green line), respectively. The non-linear relationship was also performed (solid, red line and solid, green line) and are compared with linear-relation and experimental data.

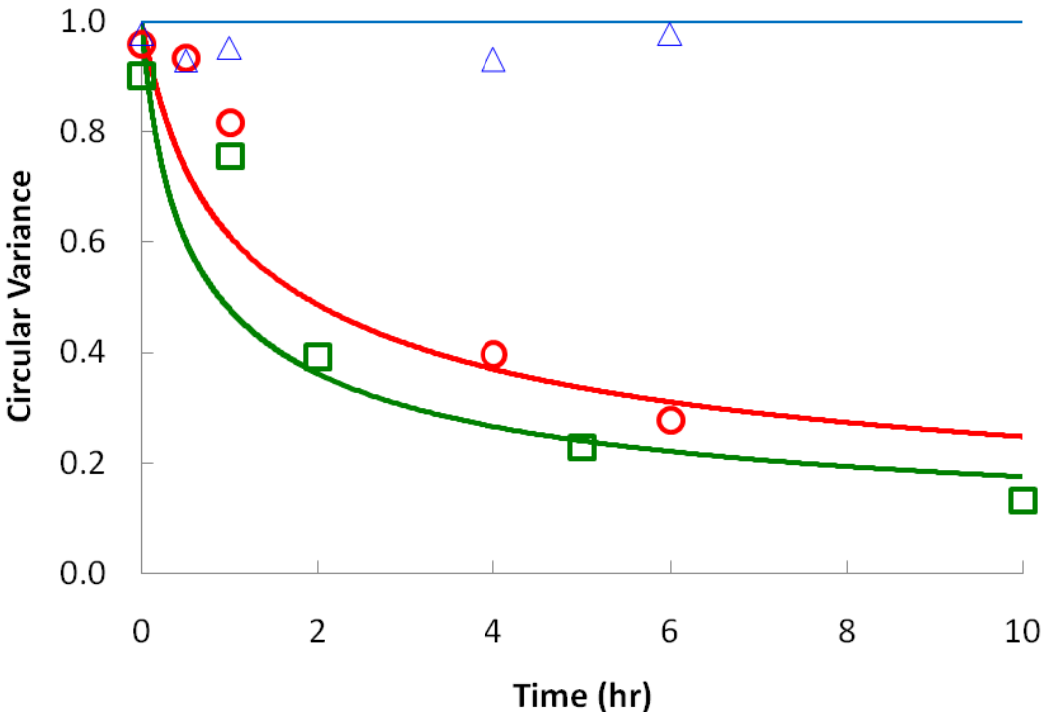

Fig. 7. Estimation of rate parameters from experimental data. Circular variances published by Kaunas et al. (2006) for 10%, 1 Hz cyclic uniaxial (red circles) and equibiaxial (blue triangles) stretches of confluent BAECs and Yoshigi et al. (2003) for 10%, 0.5 Hz cyclic uniaxial stretch (green squares) of confluent HUVECs were used to estimate the rate parameters. Rate parameters chose to describe the uniaxial data for Kaunas et al. were $k_0 = 10^{-6}\ s^{-1}$ and $k_1 = 2.5 \times 10^5\ s^{-1}$. The rate parameters for the data for Yoshigi et al. were $k_0 = 10^{-6}\ s^{-1}$ and $k_1 = 5.2 \times 10^5\ s^{-1}$.

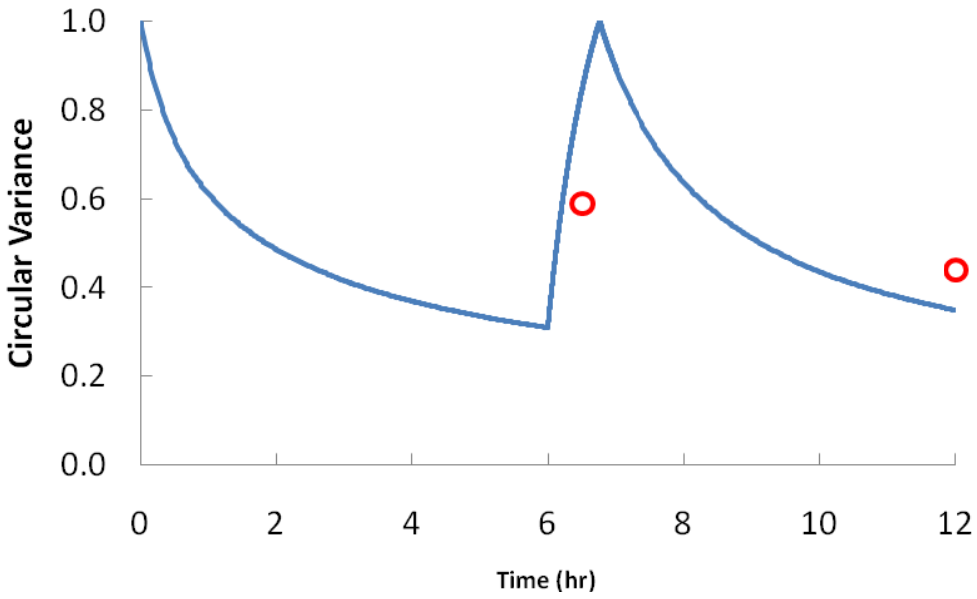

Fig. 8. Simulated responses to a changes in the direction of stretch. The predicted circular variances over time are shown for simulations of 6 hr of 10%, 1 Hz uniaxial stretch, followed by another bout of uniaxial stretch in the transverse direction for an additional 6 hr using the same rate parameters for Kaunas et al. ($k_0 = 10^{-6}\ s^{-1}$ and $k_1 = 2.5 \times 10^5\ s^{-1}$). Experimentally measured values of circular variance at different instances in the stretch regimen are shown for comparison (red circles).

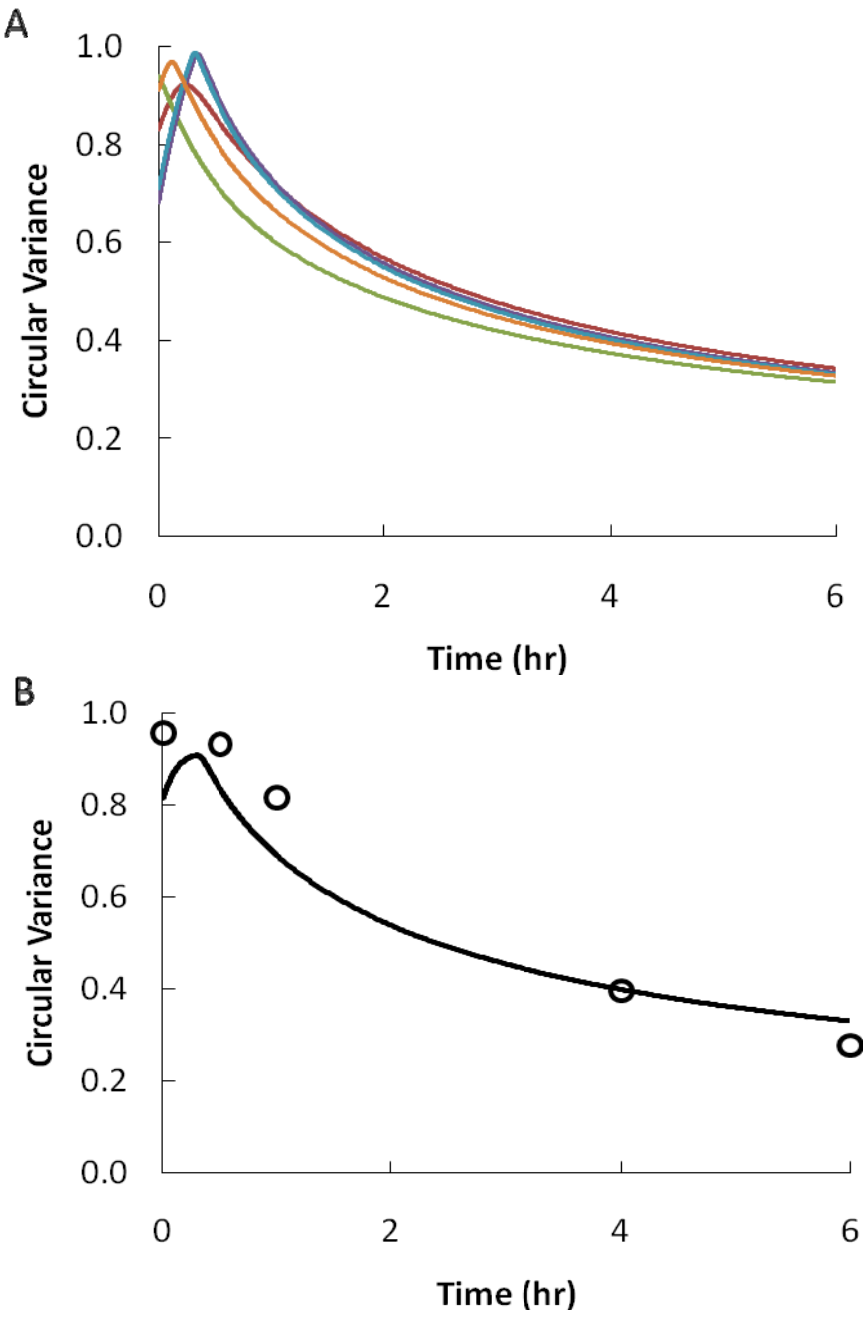

Fig. 9. The time course of stress fibers alignment under uniform and random initial mass distribution compared with experiment data. **(A)** Simulations of 10% cyclic stretch at 1 Hz were performed for experimentally measured values of initial distributions of stress fibers in five cells (data are unpublished) by parameter estimated above ($k_0 = 10^{-6}\ s^{-1}$ and $k_1 = 2.5 \times 10^5\ s^{-1}$). **(B)** The time course of the average circular variance for five cells (black line) is compared with the data for Kaunas et al. (2006).

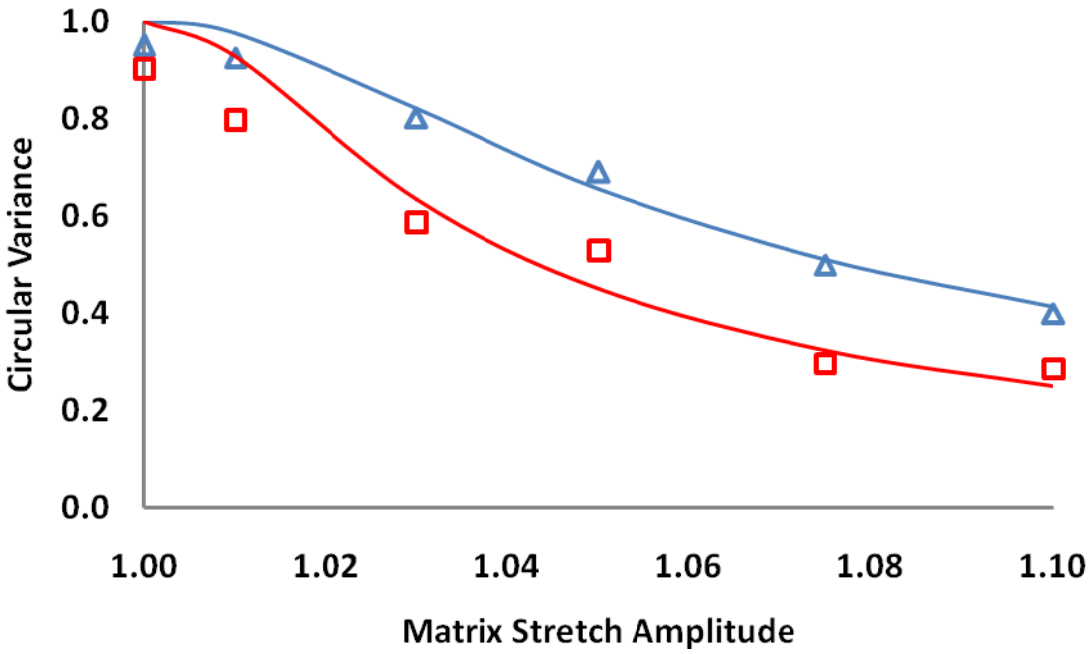

Fig. 10. Effects of active-RhoV14 expression on the estimation k_1. Circular variances published by Kaunas et al.(2005) for 1 Hz cyclic uniaxial stretch of non-confluent BAECs transfected with GFP (blue triangles) and RhoV14+GFP (red squares). Curves illustrate the model fitting for the GFP-expressing cells ($k_1 = 1.6 \times 10^5\ s^{-1}; R^2 = 0.99$) and the RhoV14-expressing cells ($k_1 = 4.0 \times 10^5\ s^{-1}; R^2 = 0.97$).

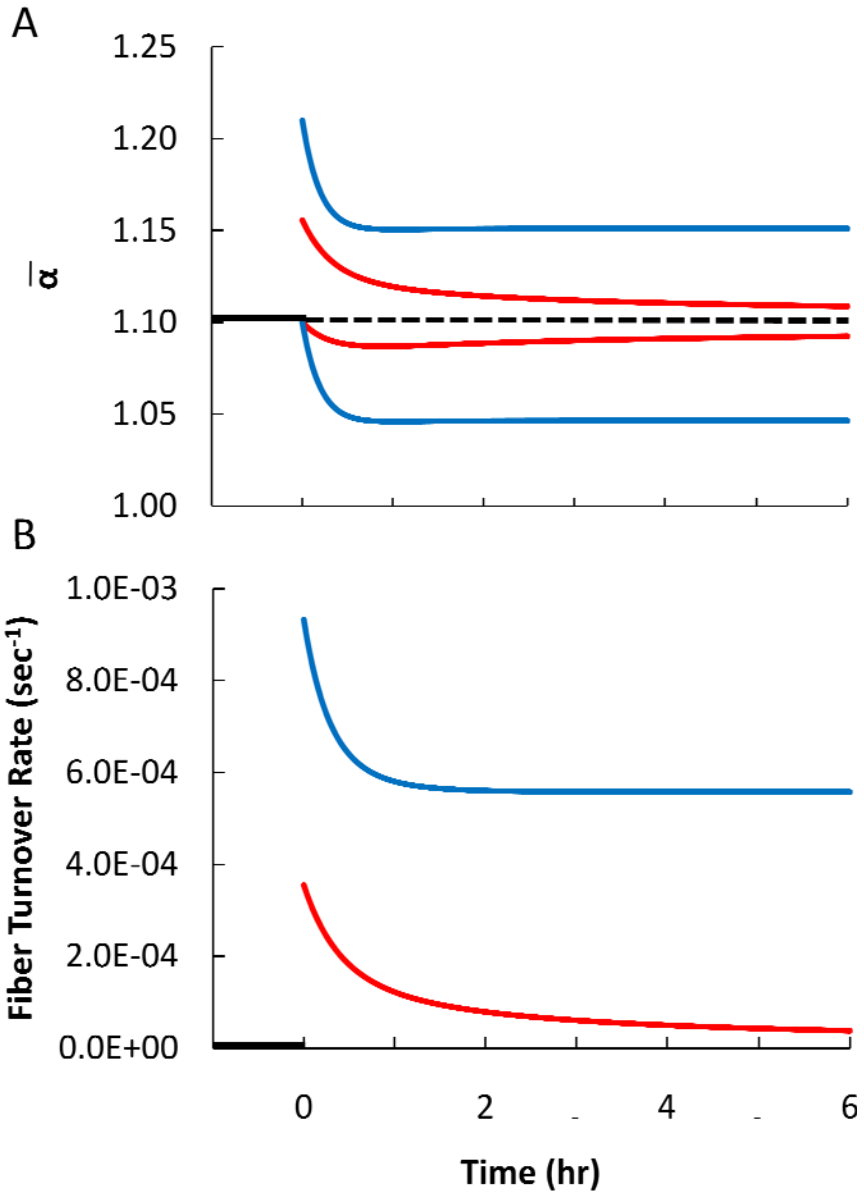

Fig. 11. Time evolution of fiber stretch and fiber turnover rate. The maximum and minimum values of $\bar{\alpha}$ during a cycle (A) and the rate of stress fiber turnover, expressed as the mass fraction of fibers disassembled per cycle (B), are shown for 10%, 1 Hz cyclic equibiaxial (blue lines) and uniaxial (red lines) stretches. The fiber stretch amplitude is the ratio of the maximum and minimum values of $\bar{\alpha}$ during a cycle. The original values for $\bar{\alpha}$ and stress fiber turnover rate before stretching are shown at $t < 0$ (black line). A dashed line indicating the value for $\bar{\alpha}$ is shown to illustrate that $\bar{\alpha}$ oscillates around this value during each cycle at steady-state.

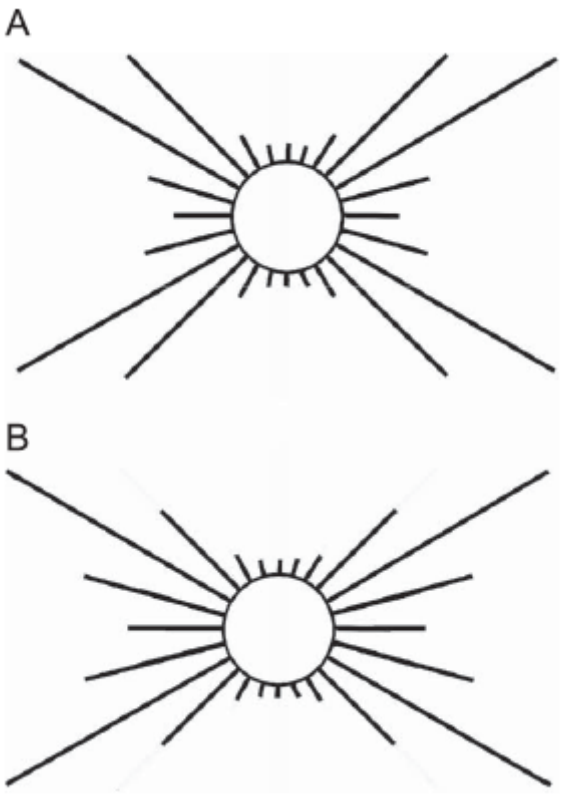

Fig. 12. In response to simple elongation, stress fibers tend to align in the direction of minimum normal matrix stretch. Simulations were performed for 10%, 1 Hz cyclic simple elongation in which the matrix contracted perpendicular to the direction of elongation (elongation was in the vertical direction in reference to the histograms). The stress fiber distributions after 6 hr of 10% simple elongation are shown for Poisson ratios of 0.35 (A) and 0.5 (B).

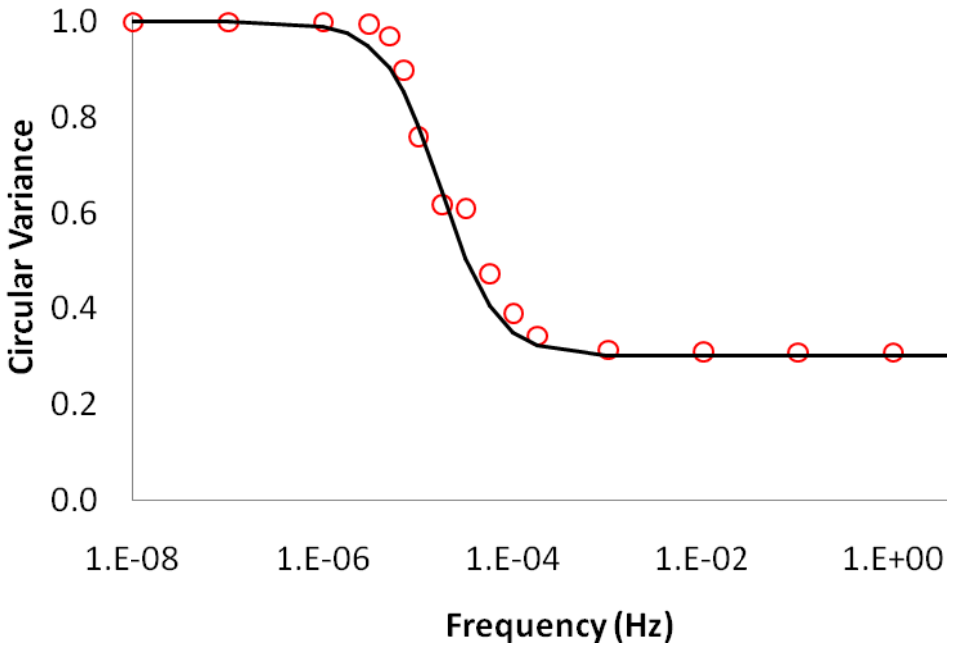

Fig. 13. Predicted effect of stretch frequency on the extent of stress fiber alignment. The effects of stretch frequency on the circular variances are shown for simulations of 10% cyclic uniaxial stretch at various frequencies at the time point of 6 hr.

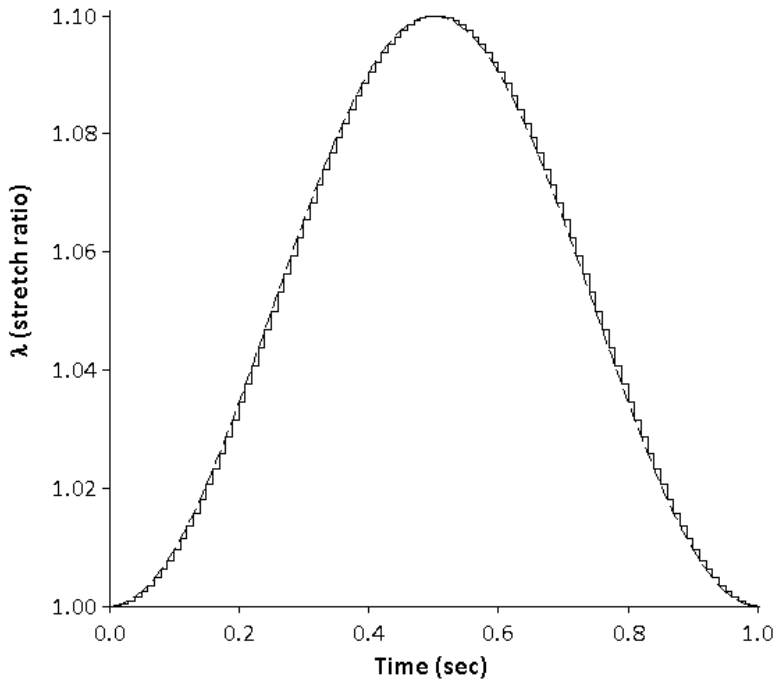

Fig. 14. Simulated sinusoidal stretch pattern. One cycle of simulation 10% cyclic sinusoidal matrix stretch at 1 Hz (solid lines) are shown with consisting of 100 steps of constant time increment (Δt=0.01 *s*). The magnitude of each step was varied to simulate a sinusoidal function.

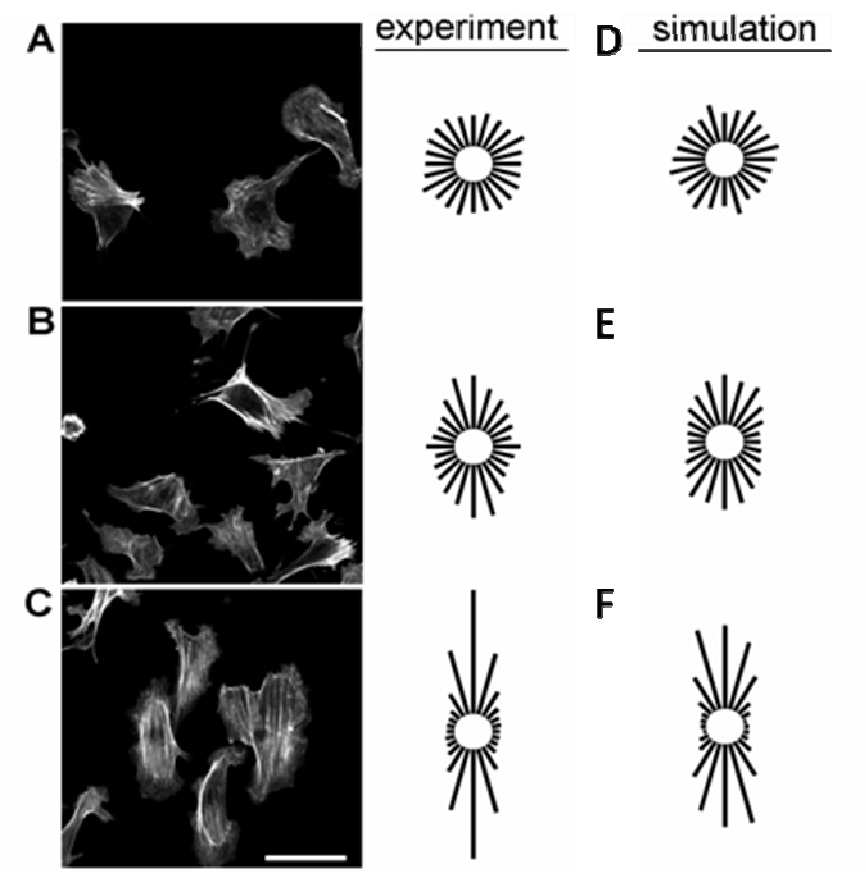

Fig. 15. The extent of stress fiber alignment depends on the frequency of cyclic uniaxial stretch. (A-C) Representative images are shown of sparsely seeded bovine aortic ECs that were subjected to 4 hr of 10% cyclic uniaxial stretch at frequencies of 0.01 (A), 0.1 (B), and 1 Hz (C), fixed, and stained for F-actin. The distributions of stress fiber orientations were determined using an intensity gradient algorithm and the results from multiple cells (n = 50 cells) are summarized as angular histograms (direction of stretch is horizontal with respect to the page). **(D-F)** Simulations of stress fiber reorganization in response to 4 hr of 10% cyclic uniaxial stretch at frequencies of 0.01 (D), 0.1 (E) and 1 Hz (F) were performed using the optimized parameter values ($k_0 = 3.0 \times 10^{-4}\ s^{-1}, k_1 = 1.7 \times 10^{4}\ s^{-1}$, and $\tau = 0.5\ s$) and the angular histograms are shown for comparison to the experimental results. Bar, 50 mm.

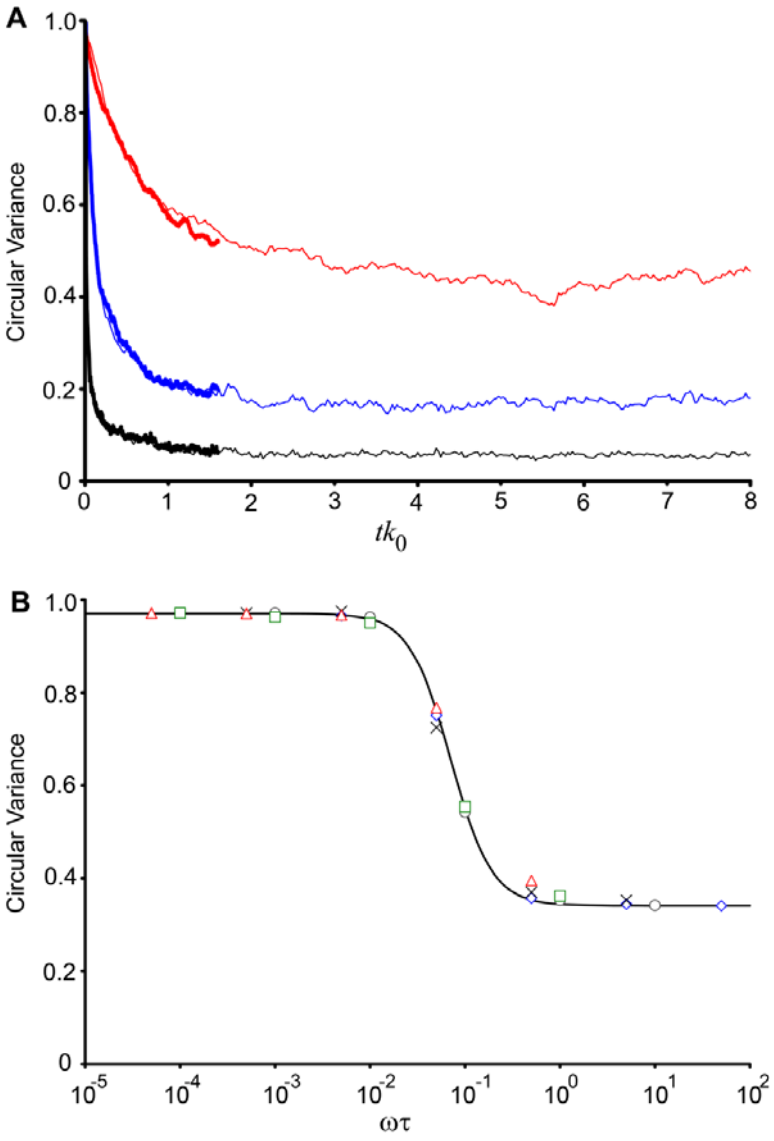

Fig. 16. Sensitivity of the system behavior to the values of the model parameters. (A) Simulations of 10% cyclic uniaxial stretch at 1 Hz were performed over a range of values for k_0 values of 10^{-4} (thick curves) and 10^{-5} s^{-1} (thin curves), and k_1 values of 10^3 (red curves), 10^4 (blue curves), and 10^5 (black curves). Circular variance was plotted versus nondimensionalized time tk_0 to illustrate that the rate of alignment scales with k_0, while the steady-state response depends on k_1. **(B)** The effects stretch frequency on the steady-state average circular variance are shown for of t values of 0.05 (triangles), 0.1 (squares), 0.5 (crossmarks), 1 (circles) and 5 s (diamonds), with k_0 and k_1 held constant at the optimized values. Plotting circular variance versus non-dimensionalized frequency illustrates that the values for the threshold and saturation frequencies scale with τ.

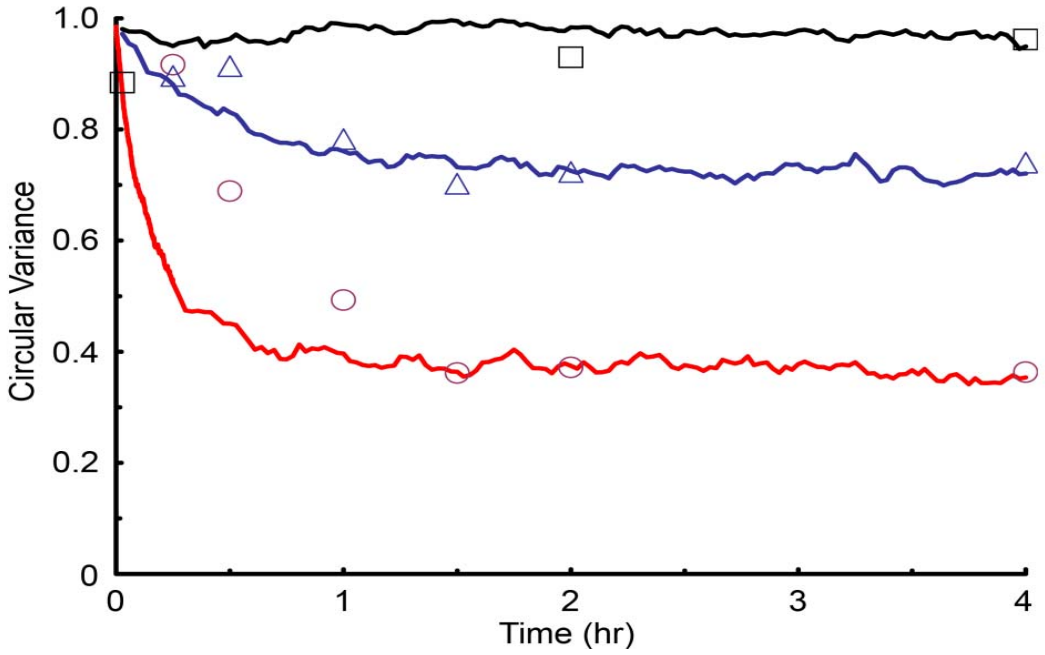

Fig. 17. Parameter estimation using the time courses of stress fiber alignment. Circular variances of the stress fiber distributions were plotted over the period indicated to show the time courses of stress fiber alignment in response to 10% cyclic uniaxial stretch at frequencies of 1 (red circles), 0.1 (blue triangles), and 0.01 Hz (black squares). Results from simulations using the optimized parameter values ($k_0 = 3.0 \times 10^{-4}\ s^{-1}, k_1 = 1.7 \times 10^{4}\ s^{-1}$, and $\tau = 0.5\ s$) are illustrated for these conditions (solid curves).

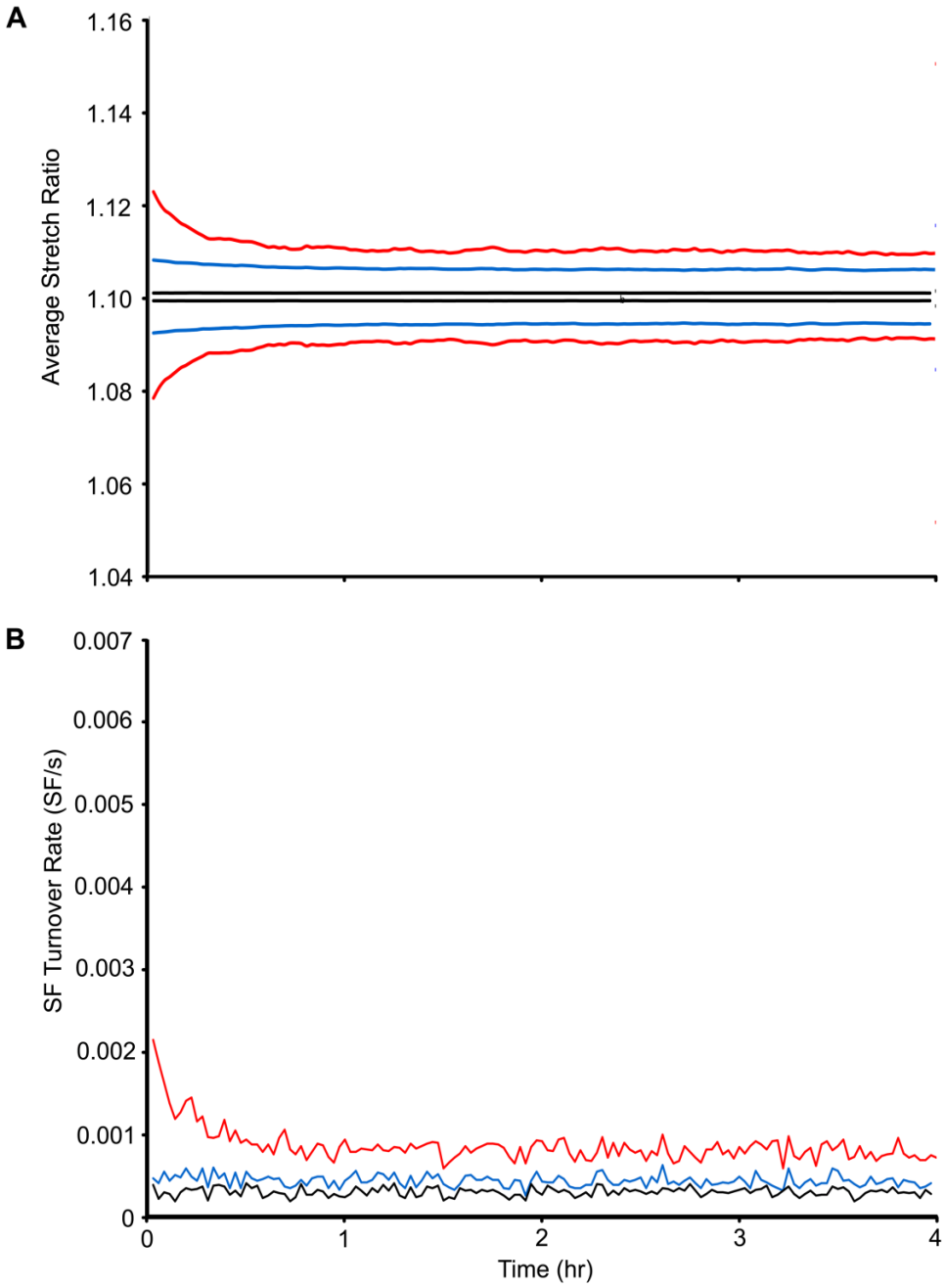

Fig. 18. Predicted time evolutions of stress fiber stretch and turnover rate in response to different frequencies of uniaxial stretch. The maximum and minimum values of the population-averaged fiber stretch during a cycle (A) and the rate of stress fiber turnover (B) are shown for simulations of 10% cyclic uniaxial stretch at frequencies of 1 (red), 0.1 (blue) and 0.01 Hz (black) using the optimized parameter values.

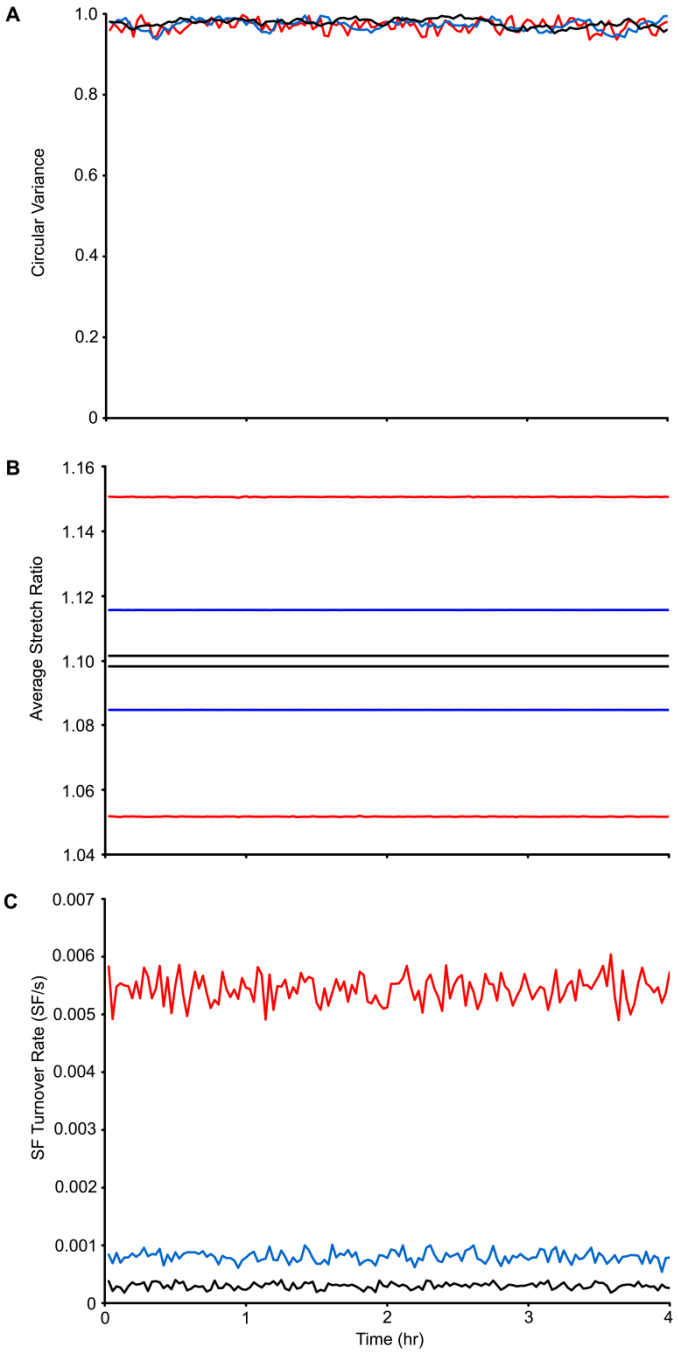

Fig. 19. Predicted time evolutions of circular variance, stress fiber stretch and fiber turnover rate in response to different frequencies of equibiaxial stretch. The circular variance (A), the maximum and minimum values of the population-averaged fiber stretch during a cycle (B), and the rate of stress fiber turnover (C) are shown for simulations of 10% cyclic equibiaxial stretch at frequencies of 1 (red), 0.1 (blue) and 0.01 Hz (black) using the optimized parameter values.

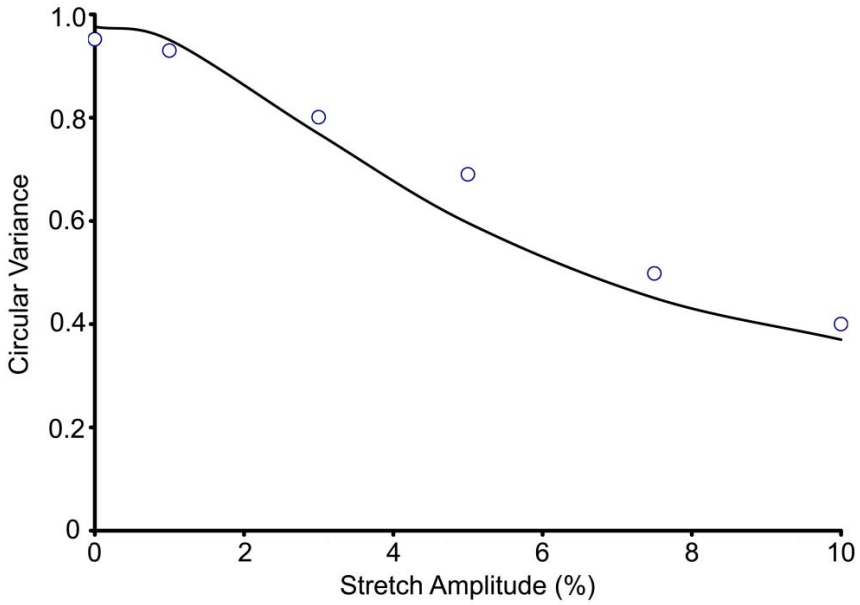

Fig. 20. Comparison between measurements and model predictions of effect of cyclic uniaxial stretch magnitude on stress fiber alignment. Simulations of 6 hr of cyclic uniaxial stretch at 1 Hz were performed over stretch magnitudes of 0 (static control) to 10% and the circular variances of the stress fiber distributions were determined using the optimized parameter values. Circular variances of experimentally measured stress fiber distributions (published in Kaunas et al. (2005)) for cyclic uniaxial stretch at 1 Hz of non-confluent bovine aortic ECs transfected with Green Fluorescent Protein (circles) are shown for comparison.

APPENDIX B. FORTRAN90 PROGRAM FOR THE DETERMINISTIC MODEL

The program is edited as .for file which can be compiled and executed by Fortran 90. The simulation data is saved in .dat file named 'DeterministicCode' and recorded as text for each cycle in the order: time, the extent of stress fiber alignment, the maximum value of fiber stretch, the minimum value of fiber stretch, and the turnover rate of stress fibers. The parameters we are interested in are q0, q1, fre, stretch, srdep, srop, duration , poisson and n, which are defined in the program and subjected to be changed.

```
!! Program name: deterministic_model.for
!! Deterministic model to perform stretch-induced stress fiber remodeling !!
implicit none
! Variable list
!----------------
! phi is the orientation of stress fibers with 5 degree intervals from  -π/2 to π/2
! c and dfgrd are Cauchy-Green tensor and the deformation gradient (F)
! faxial is the stretch in the fiber direction of the i^th constituent (α^i)
! ASR is the average stress fiber stretch in specific direction
! mass is the mass fraction of each individual family of stress fibers
! masstot is the mass summation of stress fibers in specific directions
! power is equal to 1/N
! stretch is the magnitude of cyclic stretch λ
! srinit is a constant magnitude of stretch by discretizing the magnitude of cyclic stretch λ into a
! series of N incremental stretches (λ^(1/N))
! srdep and srop are the level of fiber stretch when stress fibers reassemble  and the homeostatic level of
! fiber stretch (α_0)
! dev is the normalized deviation of stress fiber stretch (delta_α^i)
! q0 and q1 is the model parameter k_0 and k1 determining the rate and extent of stress fiber alignment
! qtheta is k^i
! poisson is the poisson ratio (ν)
! MassDisassemble is the mass fraction of disassembled stress fibers in every step
! masssum is the summation of all stress fibers
! MassTurnover is the summation of disassembled stress fibers in every cycle
! CircularVariance is the extent of stress fiber orientation
! ASRmin and ASRmax are the minimum and maximum value of fiber stretch in each cycle
! ASRsum is the average stress fiber stretch
! t is the simulation time point
! dtt is the variation of time interval for sinusoidal pattern of cyclic matrix stretch
! fre and duration are the frequency and hour of stretch
! cyclenum: the total cycle number of cyclic stretch
! ntheta is the total numbers of orientation
! k1 and n1 present specific orientation and reference configuration
! n is N steps

dimension phi(36), dfgrd(2,2), c(2,2), faxial(36,40001)
dimension ASR(36), masstot(36), mass(36,40001)
dimension tt(400), dtt(400)
real*8 pi, c, phi, dfgrd, power, stretch, srinit, srdep, srop,  faxial
real*8 dev, q0, q1, qtheta, poisson
real*8 MassDisassemble, mass, masstot, masssum, MassTurnover
real*8 etacos, etasin, CircularVariance
real*8 ASRmin, ASRmax, ASRsum, ASR
```

```
real*8 t, tt, dtt,  fre, duration, cyclenum
integer*4 ntheta, k1, i, j, m
integer*4 n, n1, n2, n3, cycle
parameter (ntheta = 36, n = 20, duration = 6.0, fre = 1.0)
parameter (stretch = 1.1, srdep = 1.1, srop = 1.1)
parameter (q0 = 0.000001, q1 = 250000, poisson = 0.0)

 cyclenum = duration*fre*3600
 pi = 2.0*asin(1.0)
 t = 0.0
 power=1.0 / n
 srinit = stretch**power

!!  Open the data file named DeterministicCode.dat to record data !!
 open (unit=1, FILE='DeterministicCode.dat', STATUS='old')
!! create titles for simulation results in each colume !!
 write (unit=1, fmt=*) "t"," Circular_Variance"," ASR(max)"," ASR(min)"," stress_fiber_turnover"

!! create 36 angle bins between -90 and +90 degrees (every 5 deg) !!
!! before stretching all fibers are uniformly distributed and in unstretched configuration !!
 do k1 = 1,ntheta
    phi(k1) = -pi/2.0 + real((k1-1))*pi/real(ntheta)
    masstot(k1) = 0.0
    do n1 = 1,2*n+1
       mass(k1,n1) = 0.0
       masstot(k1) = masstot(k1) + mass(k1,n1)
   enddo
   mass(k1,n+1) = 1.0/ntheta     !! stress fibers in traction free configuration  !!
 enddo

!! create greens deformation gradient tensor for step stretch  !!
!! calculate axial strain ratio in stretched fibers !!
 do k1 = 1,ntheta
    do n1 = 1,2*n+1
       dfgrd(1,1) = srinit**(n1-n-1)
       dfgrd(1,2) = 0.0
       dfgrd(2,1) = 0.0
       dfgrd(2,2) = 1.0-poisson*(srinit**(n1-n-1)-1.0)
    ! dfgrd(1,1) = srinit**(n1-n-1)         !! Equibiaxial stretch !!

     !! calculate greens deformation tensor !!
      do i = 1,2
        do j = 1,2
           c(i,j) = 0.0
           do m = 1,2
              c(i,j) = c(i,j)+ dfgrd(m,i)*dfgrd(m,j)
           enddo
        enddo
      enddo
      faxial(k1,n1) = cos(phi(k1))**2*c(1,1) + cos(phi(k1))*sin(phi(k1))*c(1,2)
      faxial(k1,n1) = faxial(k1,n1) + sin(phi(k1))**2*c(2,2)
      faxial(k1,n1) = faxial(k1,n1)**0.5*srdep
    enddo
 enddo

!! calculate each dt value for the same amount increase in sinusoidal wave and save as a matrix dtt !!
```

```
tt(1) = (asin((stretch**(1.0/n)-(1.0+stretch)/2.0)/((stretch-1.0)/2.0)) + asin(1.0))/(2.0*pi*fre)
do n1 = 2,(n-1)
    tt(n1) = (asin((srinit**n1-(1.0+stretch)/2.0)/((stretch-1.0)/2.0)) + asin(1.0))/(2.0*pi*fre)
    dtt(n1) = tt(n1)-tt(n1-1)
enddo
dtt(1) = (asin((stretch**(1.0/n)-(1.0+stretch)/2.0)/((stretch-1.0)/2.0)) + asin(1.0))/(2.0*pi*fre)
tt(n) = 0.5/fre
dtt(n) = tt(n) - tt(n-1)

!! create each cyclic cycle composed of n steps of stretch and n steps of release !!
n3 = 1.0
do cycle = 1,cyclenum
   MassTurnover = 0.0
   ASRmin = stretch*srdep
   ASRmax = 0.0

  !! create n steps of stretch !!
  do n2 = 1,n
     t = t + dtt(n2)
     do k1=1,ntheta
        do n1 = 2*n+1,2,-1
        mass(k1,n1) = mass(k1,n1-1)
        enddo
        mass(k1,1) = 0.0
        ASR(k1) = 0.0
        masstot(k1) = 0.0
        do n1 = 1,2*n+1
           ASR(k1) = ASR(k1) + mass(k1,n1)*faxial(k1,n1)
           masstot(k1) = masstot(k1) + mass(k1,n1)
        enddo
        ASR(k1) = ASR(k1)/masstot(k1)
     enddo

     !! calculate how much the stretched fibers disappear !!
     MassDisassemble = 1.0
     do k1 = 1,ntheta
        do n1 = 1,2*n+1
           dev = (faxial(k1,n1)-srop)/srop
           qtheta = q0*(1 + q1*dev**2)
           mass(k1,n1) = mass(k1,n1)*exp(-1*dtt(n2)*qtheta)
           MassDisassemble = MassDisassemble - mass(k1,n1)
        enddo
     enddo
     ! write (unit=1, fmt=*)  t,MassDisassemble
     MassTurnover = MassTurnover + MassDisassemble

     !! redistribute g-actin into newly deposited fibers
     ASRsum = 0.0
     do k1 = 1,ntheta
        !! uniform distribution to all fiber directions !!
        mass(k1,n+1) = mass(k1,n+1) + MassDisassemble/ntheta
        ASR(k1) = 0.0
        masstot(k1) = 0.0
        do n1 = 1,2*n+1
           ASR(k1) = ASR(k1)+ mass(k1,n1)*faxial(k1,n1)
           masstot(k1) = masstot(k1) + mass(k1,n1)
```

```
            ASRsum = ASRsum + mass(k1,n1)*faxial(k1,n1)
          enddo
          ASR(k1) = ASR(k1)/masstot(k1)
        enddo

        !! check the total mass fraction of stress fibers remains constant and is unity over time !!
        masssum = 0.0
        do k1 = 1,ntheta
          do n1 = 1,2*n+1
            masssum = masssum + mass(k1,n1)
          enddo
        enddo
        ! write (unit=1, fmt=*)  t,masssum

        !! calculate the maximum and minimum of average stress fiber stretch in each cycle !!
        if (ASRsum > ASRmax) THEN
          ASRmax = ASRsum
        else
          ASRmax = ASRmax
        endif

        if (ASRsum < ASRmin) THEN
          ASRmin = ASRsum
        else
          ASRmin = ASRmin
        endif

      enddo                    !! finish n steps of stretch !!



      !! create n steps of release !!

       do n2 = 1,n
          t = t + dtt(-n2+n+1)
          do k1 = 1,ntheta
            do n1 = 1,2*n
            mass(k1,n1) = mass(k1,n1+1)
            enddo
            mass(k1,2*n+1) = 0.0
            ASR(k1)=0.0
            masstot(k1) = 0.0
            do n1 = 1,2*n+1
              ASR(k1) = ASR(k1) + mass(k1,n1)*faxial(k1,n1)
              masstot(k1) = masstot(k1) + mass(k1,n1)
            enddo
            ASR(k1)=ASR(k1) / masstot(k1)
          enddo

          !! calculate how much the stretched fibers disappear !!
          MassDisassemble = 1.0
          do k1 = 1,ntheta
            do n1 = 1,2*n+1
              dev = (faxial(k1,n1)-srop) / srop
              qtheta = q0*(1 + q1*dev**2)
```

```
            mass(k1,n1) = mass(k1,n1)*exp(-1*dtt(-n2+n+1)*qtheta)
            MassDisassemble = MassDisassemble - mass(k1,n1)
          enddo
        enddo
        ! write (unit=1, fmt=*)  t, MassDisassemble
        MassTurnover = MassTurnover + MassDisassemble

        !! redistribute g-actin into newly deposited fibers !!
        ASRsum = 0.0
        do k1 = 1,ntheta
          !! uniform distribution to all fiber directions !!
          mass(k1,n+1) = mass(k1,n+1) + MassDisassemble/ntheta
          ASR(k1) = 0.0
          masstot(k1) = 0.0
          do n1 = 1,2*n+1
            ASR(k1) = ASR(k1) + mass(k1,n1)*faxial(k1,n1)
            masstot(k1) = masstot(k1) + mass(k1,n1)
            ASRsum = ASRsum + mass(k1,n1)*faxial(k1,n1)
          enddo
          ASR(k1) = ASR(k1) / masstot(k1)
        enddo

        !! check the total mass fraction of stress fibers remains constant and is unity over time !!
         masssum = 0.0
         do k1 = 1,ntheta
            do n1 = 1,2*n+1
               masssum = masssum + mass(k1,n1)
            enddo
         enddo
         ! write (unit=1, fmt=*)  t,masssum

        !! calculate the maximum and minimum of average stress fiber stretch in each cycle !!
         if (ASRsum > ASRmax) THEN
           ASRmax = ASRsum
         else
           ASRmax = ASRmax
         endif

         if (ASRsum < ASRmin) THEN
           ASRmin = ASRsum
         else
            ASRmin = ASRmin
         endif

    enddo                       !! finish n steps of release !!

    !! record data for each cycle in first 3600 cycles and for each 60 cycles after 3600 cycles!!
    if (cycle <= 3600) THEN
      ASRsum = 0.0
      etacos = 0.0
      etasin = 0.0
      do k1 = 1,ntheta
         ASR(k1) = 0.0
         masstot(k1) = 0.0
        do n1 = 1,2*n+1
            ASR(k1) = ASR(k1) + mass(k1,n1)*faxial(k1,n1)
```

```
            masstot(k1) = masstot(k1) + mass(k1,n1)
            etacos = etacos + cos(2.0*phi(k1))*mass(k1,n1)
            etasin = etasin + sin(2.0*phi(k1))*mass(k1,n1)
            ASRsum = ASRsum + mass(k1,n1)*faxial(k1,n1)
          enddo
          ASR(k1) = ASR(k1) / masstot(k1)
          ! write (unit=1, fmt=*)  t,phi(K1),masstot(K1),ASR(K1)
        enddo
        CircularVariance = 1 - sqrt(etacos**2.0+etasin**2.0)
         write (unit=1, fmt=*)  t,CircularVariance,ASRmax,ASRmin,MassTurnover*fre
         n3 = cycle / 60 + 1
      else
         if (cycle / 60 == n3) THEN
           etacos = 0.0
           etasin = 0.0
           ASRsum = 0.0
          do k1 = 1,ntheta
             ASR(k1) = 0.0
             masstot(k1) = 0.0
             do n1 = 1,2*n+1
                ASR(k1) = ASR(k1) + mass(k1,n1)*faxial(k1,n1)
                masstot(k1) = masstot(k1) + mass(k1,n1)
                etacos = etacos + cos(2.0*phi(k1))*mass(k1,n1)
                etasin = etasin + sin(2.0*phi(k1))*mass(k1,n1)
                ASRsum = ASRsum + mass(k1,n1)*faxial(k1,n1)
             enddo
             ASR(k1) = ASR(k1)/masstot(k1)
             ! write (unit=1, fmt=*)  t,phi(k1),masstot(k1),ASR(k1)
          enddo
          CircularVariance =1 - sqrt(etacos**2.0 + etasin**2.0)
          write (unit=1, fmt=*)  t,CircularVariance,ASRmax,ASRmin,MassTurnover*fre
          n3 = n3+1
         end if
      end if                      !! finish data record for one cycle!!

    enddo                       !! finish one cycle !!

!! close the output file !!
close (unit=1)
end
```

APPENDIX C. VISUAL C++ PROGRAM FOR THE STOCHASTIC MODEL

The program is edited in .cpp file which can be compiled and executed by Visual C++ compiler. The output data is saved in .txt file named 'file.txt' and 'histogram.txt'. The simulation results are recorded in 'file.txt' for every 100 seconds in the order: time, the maximum value of fiber stretch, the minimum value of fiber stretch, the extent of stress fiber alignment, and the turnover rate of stress fibers, while 'histogram.txt' records the distribution of stress fibers at 4 hr. The parameters we are interested in are q0, q1, tvisc, fre, stretch, srdep, and srop, which are defined in the program. Since Visual C++ cannot generate real random numbers between 0 and 1, we employ 'rng_mt.cpp' which is a random number generator program.

```
// q is fiber stretch in each individual stress fibers
// x is the value of fiber stretch after the self-adjustment activity
// theta is the angle of stress fibers generated by rng_mt
// dfgrd is the deformation gradient (F)
// Histogram is the angle of stress fibers at 4 hr
// SFangle is the distribution of stress fibers with 15 degree intervals from  -π/2 to π/2
// MassTurnover is  the summation of disassembled stress fibers for every 100 sec
// turnover_rate is the average turnover rate of stress fibers for every 100 sec
// CircularVariance: the extent of stress fiber alignment
// freq is frequency
// sr, srv, and are α0, αi, and ki
// ASRmax and ASRmin are the maximum and minimum value of fiber stretch in each cycle
// p is random number
// probability: the probability that a particular stress fiber existing at time t  disassemble at time t+dt
// str_inc is every small incremental magnitude of stretch λ
// srdep is the level of fiber stretch when stress fibers reassemble
// srop is the homeostatic level of fiber stretch (α)
// SFnum is the numbers of stress fibers in individual cells
// tvisc is the time constant of stress fiber self-adjustment
// dt is a fixed increment time
// cyclenum is total cycle number for each simulation = duration * 3600 (sec) * frequency


#Program name: statisticsinf.cpp
#include<fstream>
#include<stdio.h>
#include<stdlib.h>
#include<math.h>
#include<ctime>
#include <cstdio>
#include <cmath>

#define PI 3.141592653589793
using namespace std;

void init_genrand(unsigned long s);
void init_by_array(unsigned long init_key[], unsigned long key_length);
unsigned long genrand_int32(void);
long genrand_int31(void);
```

```
double genrand_real1(void);
double genrand_real2(void);
double genrand_real3(void);
double genrand_res53(void);

long double square(long double x);
int main(int argc, char *argv[]){
        long double  q[1000][2], x[2][1], theta[1][1000];
        long double  dfgrd[2][2], Histogram[1][1000];
        int SFangle[12] = {0};
        int i,j, m, n2, MassTurnover, OutputNo, cycleper100int, cycle, cycleper100sec;
        double turnover_rate[5001][1], CircularVariance[5001][1];
        long double  freq = 1.0;
        long double  sr, srv, ASRmax, ASRmin;
        long double  k, p, probability, z;
        long double  str_inc, stretch = 1.1, srop = 1.1, srdep = 1.1, etacos, etasin;
        long double  k1 = 17000.0, k0 = 0.0003, SFnum = 1000.0, tvisc = 0.5;
        long double  dt = 0.01, t, steps = 0.5/freq/dt, str_t[5001], cyclenum = 4.0*3600*freq;



        ofstream outfile;
        outfile.open("file.txt");
        srand( (unsigned)time(0) );
        unsigned long init[4] = {0x123, 0x234, 0x345, 0x456}, length = 4;
        init_by_array(init, length);
        cycleper100sec = 100 * freq;
        cycleper100int = cycleper100sec;

        outfile<<"tvisc="<<tvisc<<" "<<"k0="<<k0<<" "<<"k1="<<k1<<" "<<"freqency="<<freq<<endl;

        // Simulations //
        for(j = 0; j < 1; j++){
                OutputNo = 0;
                etacos = 0.0;
                etasin = 0.0;
                MassTurnover = 0.0;
                t = 0.0;
                sr = 0.0;
                for(i = 0; i < SFnum ; i++){
                        theta[j][i] = PI * genrand_real1();     // theta is a random function between 0 and PI //
                        q[i][0] = srdep * cos(theta[j][i]);
                        q[i][1] = srdep * sin(theta[j][i]);
                        z = atan(q[i][1]/q[i][0]);
                        etacos = etacos + cos(2.0*z);
                        etasin = etasin + sin(2.0*z);
                        sr = sr + sqrt(square(q[i][0]) + square(q[i][1]));
                        // outfile<<i<<" "<<theta[j][i]<<endl;
                        if(theta[j][i] > PI){
                                printf("theta error\n");
                        }
                }
                sr = sr/SFnum;
                ASRmax = sr;
                ASRmin = sr;
                CircularVariance[OutputNo][j] = 1.0 - sqrt(square(etacos)+square(etasin))/SFnum;
                   turnover_rate[OutputNo][j] = MassTurnover * freq / cycleper100int / SFnum;
                printf("etacos = %15.12f, etasin = %15.12f, CircularVariance = %15.12f \n", etacos, etasin,
                        CircularVariance[0][j]);
                outfile<<"time(sec)"<<" "<<"ASR(max)"<<" "<<"ASR(min)"<<" "<<"Circular_Variance"<<"
                          "<<"Turnover_rate"<<endl;
                outfile<<t<<" "<<ASRmax<<" "<<ASRmin<<" "<<CircularVariance[OutputNo][j]<<"
```

```
                "<<turnover_rate[OutputNo][j]<<endl;                    // write to file.txt //


for(cycle = 1; cycle <= cyclenum; cycle++){
        ASRmax = 0.0;
        ASRmin = stretch * srop;
        // create n steps of stretch //
        str_t[0] = srdep;
        for(n2 = 1; n2 <= steps; n2++){
                t = t + dt;
                str_t[n2] = (srdep * (stretch-1.0)/2.0) * (sin(2*PI*freq*t - PI/2.0)+ 1.0 ) + 1.1;
                str_inc = str_t[n2] / str_t[n2-1];
                // create greens deformation gradient tensor for step stretch  //
                dfgrd[0][0] = str_inc;
                dfgrd[0][1] = 0.0;
                dfgrd[1][0] = 0.0;
                dfgrd[1][1] = 1.0;
                // stretch all fibers one increment
                for(i = 0; i < SFnum; i++){
                        // calculate axial strain ratio in stretched fibers
                        x[0][0] = dfgrd[0][0]*q[i][0] + dfgrd[0][1]*q[i][1];
                        x[1][0] = dfgrd[1][0]*q[i][0] + dfgrd[1][1]*q[i][1];
                        sr = sqrt(square(x[0][0]) + square(x[1][0]));
                        srv = srop + (sr - srop) * exp(-dt/tvisc);
                        x[0][0] = x[0][0]*srv/sr;
                        x[1][0] = x[1][0]*srv/sr;
                        k = k0 * (1 + k1 * square((srv-srop)/srop));
                        q[i][0] = x[0][0];
                        q[i][1] = x[1][0];
                        p = genrand_res53();
                        probability = k*dt;
                        if(p>1.0){
                                printf("p error\n");
                        }

                        if (p <= probability) {
                                theta[j][i] = genrand_real1();
                                theta[j][i] = PI*theta[j][i];
                                q[i][0] = srdep * cos(theta[j][i]);
                                q[i][1] = srdep * sin(theta[j][i]);
                                MassTurnover = MassTurnover + 1;
                                if(theta[j][i] > PI){
                                        printf("theta error\n");
                                }
                        }

                        if (cycle == 4.0 * 3600 * freq){
                                z = atan(q[i][1]/q[i][0]);
                                Histogram[j][i] = z;
                        }
                }

                sr = 0.0;
                for(i = 0; i < SFnum; i++){
                        sr = sr + sqrt(square(q[i][0]) + square(q[i][1]));
                }
                sr = sr/SFnum;
                if(sr > ASRmax){
                        ASRmax = sr;
                }
                else{
```

```
                ASRmax = ASRmax;
        }
        if(sr < ASRmin){
                ASRmin = sr;
        }
        else{
                ASRmin = ASRmin;
        }
}

// create n steps of release //
str_t[0] = srdep*stretch;
for(n2 = 1; n2 <= steps; n2++){
        t = t + dt;
        str_t[n2] = (srdep * (stretch-1.0)/2.0) * (sin(2*PI*freq*t - PI/2.0) + 1.0) + 1.1;
        str_inc = str_t[n2]/str_t[n2-1];
        // create greens deformation gradient tensor for step release  //
        dfgrd[0][0] = str_inc;
        dfgrd[0][1] = 0.0;
        dfgrd[1][0] = 0.0;
        dfgrd[1][1] = 1.0;
        // stretch all fibers one increment
        for(i = 0; i < SFnum; i++){
                // calculate axial strain ratio in stretched fibers
                x[0][0] = dfgrd[0][0]*q[i][0] + dfgrd[0][1]*q[i][1];
                x[1][0] = dfgrd[1][0]*q[i][0] + dfgrd[1][1]*q[i][1];
                sr = sqrt(square(x[0][0])+square(x[1][0]));
                srv = srop + (sr - srop)*exp(-dt/tvisc);
                x[0][0] = x[0][0]*srv/sr;
                x[1][0] = x[1][0]*srv/sr;
                k = k0 * (1 + k1*square((srv-srop)/srop));
                q[i][0] = x[0][0];
                q[i][1] = x[1][0];
                p = genrand_res53();
                probability = k*dt;
                if(p>1.0){
                        printf("p error\n");
                }
                if (p <= probability){
                        theta[j][i] = genrand_real1();
                        theta[j][i] = PI*theta[j][i];
                        q[i][0] = srdep*cos(theta[j][i]);
                        q[i][1] = srdep*sin(theta[j][i]);
                        MassTurnover = MassTurnover + 1;
                        if(theta[j][i]>PI){
                                printf("theta error\n");
                        }
                }

                if (cycle == 4.0*3600*freq){
                        z = atan(q[i][1]/q[i][0]);
                        Histogram[j][i] = z;
                }
        }
        sr = 0.0;
        for(i = 0; i < SFnum; i++){
                sr = sr + sqrt(square(q[i][0]) + square(q[i][1]));
        }
        sr = sr/SFnum;
        if(sr > ASRmax){
                ASRmax = sr;
        }
```

```
                                        else{
                                                ASRmax = ASRmax;
                                        }
                                        if(sr < ASRmin){
                                                ASRmin = sr;
                                        }
                                        else{
                                                ASRmin = ASRmin;
                                        }
                                }

                                etacos = 0.0;
                                etasin = 0.0;
                                for(i = 0;i<SFnum;i++){
                                        z = atan(q[i][1]/q[i][0]);
                                        etacos = etacos + cos(2.0*z);
                                        etasin = etasin + sin(2.0*z);
                                }

                                // record data for each 100 seconds //
                                if(cycle % cycleper100int == 0){
                                        OutputNo = OutputNo + 1;
                                        CircularVariance[OutputNo][j] = 1.0 - sqrt(square(etacos) +
                                             square(etasin))/SFnum;
                                        // Calculate tunrover rate //
                                        turnover_rate[OutputNo][j] = MassTurnover * freq / cycleper100int / SFnum;
                                        MassTurnover = 0;
                                       //printf("cycle: %d, ASRmax: %f, ASRmin: %f, CircularVariance: %f \n",cycle,
                                                ASRmax, ASRmin, CircularVariance[OutputNo][j]);
                                        outfile<<t<<" "<<ASRmax<<" "<<ASRmin<<"
                                             "<<CircularVariance[OutputNo][j]<<"
"<<turnover_rate[OutputNo][j]<<endl;                                                    // write to file.txt //
                                }

                        }
                }

                outfile.close();                                        // close file.text //

                // open histogram.txt file to record the orientation of stress fibers //
                ofstream myfile("histogram.txt");
                myfile.is_open();
                for(j = 0; j<1; j++){
                        myfile<<"Repetation"<<"SFnum"<<"angle"<<endl;           // write to histogram.txt //
                        for(i = 0; i < SFnum; i++){
                                myfile<<j<<" "<<i<<" "<<Histogram[j][i]<<endl;          // write to histogram.txt //

                                if(Histogram[j][i]*180/PI >= -90.0 && Histogram[j][i]*180/PI < -82.5){
                                        SFangle[0]++;
                                }
                                else if(Histogram[j][i]*180/PI >= -82.5 && Histogram[j][i]*180/PI < -67.5){
                                        SFangle[1]++;
                                }
                                else if(Histogram[j][i]*180/PI >= -67.5 && Histogram[j][i]*180/PI < -52.5){
                                        SFangle[2]++;
                                }
                                else if(Histogram[j][i]*180/PI >= -52.5 && Histogram[j][i]*180/PI < -37.5){
                                        SFangle[3]++;
                                }
                                else if(Histogram[j][i]*180/PI >= -37.5 && Histogram[j][i]*180/PI < -22.5){
                                        SFangle[4]++;
                                }
```

```
                        else if(Histogram[j][i]*180/PI >= -22.5 && Histogram[j][i]*180/PI < -7.5){
                                SFangle[5]++;
                        }
                        else if(Histogram[j][i]*180/PI >= -7.5 && Histogram[j][i]*180/PI < 7.5){
                                SFangle[6]++;
                        }
                        else if(Histogram[j][i]*180/PI >= 7.5 && Histogram[j][i]*180/PI < 22.5){
                                SFangle[7]++;
                        }
                        else if(Histogram[j][i]*180/PI >= 22.5 && Histogram[j][i]*180/PI < 37.5){
                                SFangle[8]++;
                        }
                        else if(Histogram[j][i]*180/PI >= 37.5 && Histogram[j][i]*180/PI < 52.5){
                                SFangle[9]++;
                        }
                        else if(Histogram[j][i]*180/PI >= 52.5 && Histogram[j][i]*180/PI < 67.5){
                                SFangle[10]++;
                        }
                        else if(Histogram[j][i]*180/PI >= 67.5 && Histogram[j][i]*180/PI < 82.5){
                                SFangle[11]++;
                        }
                        else{
                                SFangle[0]++;
                        }
                }
        }
        myfile<<"SFangle"<<endl;
        for(m = 0; m < 12; m++){
                myfile<<"angle"<<-90+15*m<<" "<<SFangle[m]<<endl;      // write to histogram.txt //
        }
        myfile.close();                                         // close histogram.txt file //
        return EXIT_SUCCESS;
}


// create Square function //
long double square(long double x){
        long double y;
        y = (x)*(x);
        return y;
}
```

APPENDIX D. VISUAL C++ PROGRAM FOR RANDOM NUMBER GENERATOR

The program is edited in .cpp file which should be put in the same directory as the stochastic model. The simulation generates a random number on [0,1) with 53-bit resolution.

```
#include <cstdio>
using namespace std;

/* Period parameters */
#define N 624
#define M 397
#define MATRIX_A 0x9908b0dfUL   /* constant vector a */
#define UPPER_MASK 0x80000000UL /* most significant w-r bits */
#define LOWER_MASK 0x7fffffffUL /* least significant r bits */

static unsigned long mt[N]; /* the array for the state vector  */
static int mti=N+1; /* mti==N+1 means mt[N] is not initialized */

/* initializes mt[N] with a seed */
void init_genrand(unsigned long s)
{
    mt[0]= s & 0xffffffffUL;
    for (mti=1; mti<N; mti++) {
        mt[mti] =
                (1812433253UL * (mt[mti-1] ^ (mt[mti-1] >> 30)) + mti);
        /* See Knuth TAOCP Vol2. 3rd Ed. P.106 for multiplier. */
        /* In the previous versions, MSBs of the seed affect   */
        /* only MSBs of the array mt[].                        */
        /* 2002/01/09 modified by Makoto Matsumoto             */
        mt[mti] &= 0xffffffffUL;
        /* for >32 bit machines */
    }
}

/* initialize by an array with array-length */
/* init_key is the array for initializing keys */
/* key_length is its length */
//void init_by_array(init_key, key_length)
//unsigned long init_key[], key_length;
void init_by_array(unsigned long init_key[], unsigned long key_length)
{
    int i, j, k;
    init_genrand(19650218UL);
    i=1; j=0;
    k = (N>key_length ? N : key_length);
    for (; k; k--) {
        mt[i] = (mt[i] ^ ((mt[i-1] ^ (mt[i-1] >> 30)) * 1664525UL))
          + init_key[j] + j; /* non linear */
        mt[i] &= 0xffffffffUL; /* for WORDSIZE > 32 machines */
        i++; j++;
        if (i>=N) { mt[0] = mt[N-1]; i=1; }
```

```
        if (j>=key_length) j=0;
    }
    for (k=N-1; k; k--) {
        mt[i] = (mt[i] ^ ((mt[i-1] ^ (mt[i-1] >> 30)) * 1566083941UL))
          - i; /* non linear */
        mt[i] &= 0xffffffffUL; /* for WORDSIZE > 32 machines */
        i++;
        if (i>=N) { mt[0] = mt[N-1]; i=1; }
    }

    mt[0] = 0x80000000UL; /* MSB is 1; assuring non-zero initial array */
}

/* generates a random number on [0,0xffffffff]-interval */
unsigned long genrand_int32(void)
{
    unsigned long y;
    static unsigned long mag01[2]={0x0UL, MATRIX_A};
    /* mag01[x] = x * MATRIX_A  for x=0,1 */

    if (mti >= N) { /* generate N words at one time */
        int kk;

        if (mti == N+1)   /* if init_genrand() has not been called, */
            init_genrand(5489UL); /* a default initial seed is used */

        for (kk=0;kk<N-M;kk++) {
            y = (mt[kk]&UPPER_MASK)|(mt[kk+1]&LOWER_MASK);
            mt[kk] = mt[kk+M] ^ (y >> 1) ^ mag01[y & 0x1UL];
        }
        for (;kk<N-1;kk++) {
            y = (mt[kk]&UPPER_MASK)|(mt[kk+1]&LOWER_MASK);
            mt[kk] = mt[kk+(M-N)] ^ (y >> 1) ^ mag01[y & 0x1UL];
        }
        y = (mt[N-1]&UPPER_MASK)|(mt[0]&LOWER_MASK);
        mt[N-1] = mt[M-1] ^ (y >> 1) ^ mag01[y & 0x1UL];

        mti = 0;
    }

    y = mt[mti++];

    /* Tempering */
    y ^= (y >> 11);
    y ^= (y << 7) & 0x9d2c5680UL;
    y ^= (y << 15) & 0xefc60000UL;
    y ^= (y >> 18);

    return y;
}

/* generates a random number on [0,0x7fffffff]-interval */
long genrand_int31(void)
{
    return (long)(genrand_int32()>>1);
}
```

```
/* generates a random number on [0,1]-real-interval */
double genrand_real1(void)
{
   return genrand_int32()*(1.0/4294967295.0);
   /* divided by 2^32-1 */
}

/* generates a random number on [0,1)-real-interval */
double genrand_real2(void)
{
   return genrand_int32()*(1.0/4294967296.0);
   /* divided by 2^32 */
}

/* generates a random number on (0,1)-real-interval */
double genrand_real3(void)
{
   return (((double)genrand_int32()) + 0.5)*(1.0/4294967296.0);
   /* divided by 2^32 */
}

/* generates a random number on [0,1) with 53-bit resolution*/
double genrand_res53(void)
{
   unsigned long a=genrand_int32()>>5, b=genrand_int32()>>6;
   return(a*67108864.0+b)*(1.0/9007199254740992.0);
}
/* These real versions are due to Isaku Wada, 2002/01/09 added */
```

APPENDIX E. MATLAB PROGRAM FOR THE ORIENTATION OF STRESS FIBERS

The program is edited in .m file which can be compiled and executed by Matlab. Before starting the computation, put images in C:\images\ directory. Type imagename = 'filename' where filename is the name of the image file in the commend window. The file must be TIFF format, but do not include the '.tif' at the end of the filename. Run the program by typing CELL. There will be two output files named 'output.dat' and 'histogram.dat'. In the 'output.dat' file, the simulation results are recorded for the total numbers of orientation vector components (N) in the order: angle, covariance, x-position, y-position, sin(2θ)/N, cos(2θ)/N and use Eq. (7) to calculate the circular variance for each image. The plot generated by the program is the original image added with colored lines which matches the apparent orientation of fibers in each subregion. The distribution of stress fibers are saved as 'histogram.dat' and plotted as the circular histograms by Oriana 2 circular statistics software (Rockware).

```
% Variable list
% ---------------
% ARE is the side length of an interrogation box
% BUFF is the buffer around the edge of the images needed for the masks
% origI is the original image
% MX, MY are the masks in the x- and y-directions
% filtIX, filtIY are the images that was convolved with MX, MY
% X, Y are the sizes of filtIX and filtIY
% G is the size of the correlation for a pixel
% Angle is the angle of lowest gradient


namex = strcat('C:\images\',imagename,'.tif');
outname = strcat('C:\images\',imagename,'.dat');
histname = strcat('C:\images\',imagename,'HIST.dat');

clear angles;
clear image;
clear origI;
clear filtIX;
clear filtIY;
clear G;
clear Angle;
clear mean_int;

ARE=10;
BUFF=4;
limit = 0.7;
% read in image. If image is indexed then convert to greyscale
[image, map] = imread(namex);
if (map)
```

```
    bwimage = ind2gray(image,map);
    origI=double(bwimage);
else
    origI=double(image);
end;
X = size(origI,2);
Y = size(origI,1);

% make masks
for i=-BUFF:BUFF
    for j=-BUFF:BUFF
        MX(i+1+BUFF,j+1+BUFF)= j/2*exp(-(i^2+j^2)/4);
        % MY(i+1+BUFF,j+1+BUFF)= i/2*exp(-(i^2+j^2)/4);
    end;
end;

% convolve image with masks. filtIX measures gradients in the x-direction,
% while filtIY measures gradients in the y-direction. Thus vertical lines
% give high values in filtIX, while horizontal lines give high values in
% filtIY.
filtIX=double(imfilter(origI,MX,'conv'));
filtIY=double(imfilter(origI,MX','conv'));
%filtIX=filtIX(:,:,3);
%filtIY=filtIY(:,:,3);

for i=1:BUFF
    filtIX(:,X-BUFF+1)=[];
    filtIY(:,X-BUFF+1)=[];
    filtIX(Y-BUFF+1,:)=[];
    filtIY(Y-BUFF+1,:)=[];
end;
for i=1:BUFF
    filtIX(:,1)=[];
    filtIY(:,1)=[];
    filtIX(1,:)=[];
    filtIY(1,:)=[];
end;
% compute metrics for convolved matrices
G=(filtIX.^2+filtIY.^2).^0.5;
filtIX=filtIX+0.0000001;
Angle=atan(filtIY./filtIX);
meanG=mean(mean(G,2));
meanAngle=mean(mean(Angle,2));
fprintf('avg. G: %6.2f \n',meanG);
fprintf('avg. angle: %6.2f \n',meanAngle*180/pi);

% compute metrics for individual features
threshold = mean(mean(origI,2))/limit;
features=1;
%step through image for each feature
for k = (1+ARE):(2*ARE):(Y-ARE-1-2*BUFF)
    for l = (1+ARE):(2*ARE):(X-ARE-1-2*BUFF)
        AMAX=90;
        ACMAX=0;
        AChold=0;
```

```
      CORATMX=0;

      % feature mean intensity and continue if it is higher then
      % threshold
      meanint = sum(sum(origI(k-ARE:k+ARE,l-ARE:l+ARE)))/(4*ARE*ARE);
      mean_int(features) = meanint;

      if (mean_int(features) > threshold)
        angles(features,3) = l;
        angles(features,4) = k;
        for m = 0:179
          aval = (m-90)*pi/180;
          AA = 0;
          CORATIO = 0;
          for i = -ARE:ARE
            for j = -ARE:ARE
              cang = Angle(k+i,l+j);
              cosval1 = exp(2*cos(2*(cang-aval)))/exp(2);
              AA = AA + G(k+i,l+j)*cosval1;
              CORATIO = CORATIO + cosval1;
            end;
          end;
          AChold = AChold + AA;
          if (AA > ACMAX)
            AMAX = m;
            ACMAX = AA;
          end;
          if (CORATIO > CORATMX)
            CORATMX = CORATIO;
          end;
        end;
      end;

      % store avg. coratio for feature with largest coratio
      angles(features,2)  = CORATMX/(4*ARE*ARE);
      % loc_dev(features) = 180/pi*(0.5-(ssin^2+scos^2)^0.5/(8*ARE*ARE))^0.5;

      % only keep this feature if the weight is high enough */
      if (mean_int(features) > threshold) && (angles(features,2) > 0.1)
        % store histogram contribution */
        angles(features,5) = angles(features,1);
        angles(features,1) = AMAX;
        fprintf('\n %d  x=%d y=%d angle=%d coratio=%6.2lf \n',...
        features,angles(features,3),angles(features,4),AMAX,angles(features,2));
        features = features + 1;
      end;
    end;
end;

features = features-1;
% save histogram and "angles" matrix to files
angleadj = angles(:,1)+2.5;
for i=1:features
    if (angleadj(i) > 180)
        angleadj(i) = angleadj(i) - 180;
```

```
    end;
end;
histo = hist(angleadj,36);

angles(:,5)=sin(angles(:,1)*2*pi/180)/features;
angles(:,6)=cos(angles(:,1)*2*pi/180)/features;

% angles stores the values for each interrogation box in a row with
%column 1 = angle, 2= covariance, 3=x-position, 4=y-position, 5=sin(2@)/N,
%column 6 = cos(2@)/N

save c:\histogram.dat histo -ASCII;
save c:\output.dat angles -ASCII;

ssin=0;
scos=0;
for i=1:features
    ssin = ssin + sin(2*angles(i,1)*pi/180);
    scos = scos + cos(2*angles(i,1)*pi/180);
end;
cmean = 0.5*atan(ssin/scos);
% adjust cmean to be in range [-pi/2,pi/2]
if (ssin > 0) && (scos < 0)
    cmean = cmean + pi/2;
end;
if (ssin < 0) && (scos < 0)
    cmean = cmean - pi/2;
end;

fprintf('\n N: %d  mean: %6.2f  SD: %6.2f \n',features, cmean*180/pi);

imshow(image);
for i=1:features-1
    if (angles(i,1)<22.5)
        line([angles(i,3)-5 angles(i,3)+5],[angles(i,4) angles(i,4)],...
            'Color',[1 0 0],'Marker','none','LineStyle','-');
    end;
    if ((angles(i,1)>22.5) && (angles(i,1)<67.5))
        line([angles(i,3)-5 angles(i,3)+5],[angles(i,4)-5 angles(i,4)+5],...
            'Color',[0 1 0],'Marker','none','LineStyle','-');
    end;
    if ((angles(i,1)>67.5) && (angles(i,1)<112.5))
        line([angles(i,3) angles(i,3)],[angles(i,4)-5 angles(i,4)+5],...
            'Color',[0 0 1],'Marker','none','LineStyle','-');
    end;
    if ((angles(i,1)>112.5) && (angles(i,1)<157.5))
        line([angles(i,3)-5 angles(i,3)+5],[angles(i,4)+5 angles(i,4)-5],...
            'Color',[1 1 0],'Marker','none','LineStyle','-');
    end;
    if (angles(i,1)>157.5)
        line([angles(i,3)-5 angles(i,3)+5],[angles(i,4) angles(i,4)],...
            'Color',[1 0 0],'Marker','none','LineStyle','-');
    end;
end;
```

VITA

Name: Hui-Ju Hsu

Address: Biomedical Engineering
c/o Dr. Roland Kaunas
Texas A&M University
College Station, TX 77843-3120

Email Address: emmeline0814@gmail.com

Education: B.S., National Cheng Kung University, Taiwan, 2004

M.S., National Cheng Kung University, Taiwan, 2006

M.S., Texas A&M, USA, 2009